# Assessment of Simulated Soil Moisture from WRF Noah, Noah-MP, and CLM Land Surface Schemes for Landslide Hazard Application

Lu Zhuo[1], Qiang Dai[1,2*], Dawei Han[1], Ningsheng Chen[3], Binru Zhao[1,4]

[1]WEMRC, Department of Civil Engineering, University of Bristol, Bristol, UK

[2]Key Laboratory of VGE of Ministry of Education, Nanjing Normal University, Nanjing, China

[3]The Institute of Mountain Hazards and Environment (IMHE), China

[4]College of Water Conservancy and Hydropower Engineering, Hohai University, Nanjing, China

[*]Correspondence: civengwater@gmail.com

## Abstract

This study assesses the usability of Weather Research and Forecasting (WRF) model simulated soil moisture for landslide monitoring in the Emilia Romagna region, northern Italy during the 10-year period between 2006 and 2015. Particularly three advanced Land Surface Model (LSM) schemes (i.e., Noah, Noah-MP and CLM4) integrated with the WRF are used to provide detailed multi-layer soil moisture information. Through the temporal evaluation with the single-point in-situ soil moisture observations, Noah-MP is the only scheme that is able to simulate the large soil drying phenomenon close to the observations during the dry season, and it also has the highest correlation coefficient and the lowest *RMSE* at most soil layers. It is also demonstrated that a single soil moisture sensor located in plain area has high correlation with a significant proportion of the study area (even in the mountainous region 141 km away, based on the WRF simulated spatial soil moisture information). The evaluation of the WRF rainfall estimation shows there is no distinct difference among the three LSMs, and their performances are in line with a published study for the central USA. Each simulated soil moisture product from the three LSM schemes is then used to build a landslide prediction model, and within each model, 17 different exceedance probably levels from 1% to 50% are adopted to determine the optimal threshold scenario (in total there are 612 scenarios). Slope degree information is also used to separate the study region into different

groups. The threshold evaluation performance is based on the landslide forecasting accuracy using 45 selected rainfall events between 2014-2015. Contingency tables, statistical indicators, and Receiver Operating Characteristic analysis for different threshold scenarios are explored. The results have shown that, for landslide monitoring, Noah-MP at the surface soil layer with 30% exceedance probability provides the best landslide monitoring performance, with its hitting rate at 0.769, and its false alarm rate at 0.289.

**Keywords:** Emilia Romagna, Weather Research and Forecasting (WRF) Model, Land Surface Model (LSM), Numerical Weather Prediction (NWP) model, landslide hazards, soil moisture.

## 1. Introduction

Landslide is a repeated geological hazard during rainfall seasons, which causes massive destructions, loss of lives, and economic damages worldwide (Klose et al., 2014). The accurate predicting and monitoring of the spatiotemporal occurrence of the landslide is the key to prevent/ reduce casualties and damages to properties and infrastructures. One of the most widely adopted methods for landslide prediction is based on rainfall threshold, which relies on building the rainfall intensity-duration curve using the information from the past landslide events (Chae et al., 2017). However, such a method in many cases is insufficient for landslide hazard assessment (Posner and Georgakakos, 2015), because in addition to rainfall, initial soil moisture condition is one of the main triggering factors of the events (Glade et al., 2000;Crozier, 1999;Tsai and Chen, 2010;Hawke and McConchie, 2011;Bittelli et al., 2012;Segoni et al., 2018b;Valenzuela et al., 2018;Bogaard and Greco, 2018).

For landslide applications, one potential soil moisture estimation method is through satellite remote sensing technologies. Although such technologies have been improved significantly over

the past decade, their retrieving accuracy is still largely affected by frozen soil conditions (Zhuo et al., 2015a), and dense vegetation coverages particularly in mountainous regions (Temimi et al., 2010); furthermore, the acquired data only covers the top few centimetres of soil. Although the more recently launched satellites such as Sentinel-1 (1 km, and 3 days resolution) has shown some promising performance of soil moisture estimation (Gao et al., 2017;Paloscia et al., 2013), its availability only covers the recent years (Geudtner et al., 2014). Those disadvantages restrict the full utilisation of satellite soil moisture products for landslide monitoring application as discussed in our previous study (Zhuo et al., 2019). In Zhuo et al. (2019), it is discussed that both the temporal and spatial resolutions of the ESA CCI satellite soil moisture product (Dorigo et al., 2017) is too coarse for landslide applications, and its data are mostly only available after the year 2002. Moreover, the shallow depth soil moisture observation from the satellite hinders the accuracy of landslide predictions. Therefore, other alternative soil moisture estimation methods need to be explored.

One emerging area relies on modelling. Some studies have used modelled soil moisture data for landslide applications (Ponziani et al., 2012;Ciabatta et al., 2016;Zhao et al., 2019a;Zhao et al., 2019b). However, to our knowledge, there is a lack of existing study using the state-of-the-art Land Surface Models (LSMs) modelled soil moisture for landslide studies, such as the Noah LSM (Ek et al., 2003) and the Community Land Model (CLM) (Oleson et al., 2010). LSMs describe the interactions between the atmosphere and the land surface by simulating exchanges of momentum, heat and water within the Earth system (Maheu et al., 2018). They are capable of simulating the most important subsurface hydrological processes (e.g., soil moisture) and can be integrated with the advanced Numerical Weather Prediction (NWP) system like WRF (Weather Research and Forecasting) (Skamarock et al., 2008) for comprehensive soil moisture estimations (i.e., through

71 the surface energy balance, the surface layer stability and the water balance equations) (Greve et
72 al., 2013). NWP-based (i.e., with integrated LSM, thereafter) soil moisture estimations have many
73 advantages, for instance their spatial and temporal resolution can be set at different scales
74 depending on the input datasets to fit various application requirements; their coverage is global,
75 and the estimated soil moisture data covers multiple soil layers (from the shallow surface layer to
76 deep root-zones); as well as a number of globally-covered data products can provide the necessary
77 boundary and initial conditions for running the models. Soil moisture estimated through such an
78 approach has been widely recognised and demonstrated in many studies, which cover a broad
79 range of applications from hydrological modelling (Srivastava et al., 2013a;Srivastava et al., 2015),
80 drought studies (Zaitchik et al., 2013), flood investigations (Leung and Qian, 2009), to regional
81 weather prediction (Stéfanon et al., 2014). Therefore, NWP-based soil moisture datasets could
82 provide valuable information for landslide applications. However, to our knowledge, relevant
83 research has never been carried out.

84 The aim of this study hence is to evaluate the usefulness of NWP modelled soil moisture for
85 landslide monitoring. Here the advanced WRF model (version 3.8) is adopted, because it offers
86 numerous physics options such as micro-physics, surface physics, atmospheric radiation physics,
87 and planetary boundary layer physics (Srivastava et al., 2015), and can integrate with a number of
88 LSM schemes, each varying in physical parameterisation complexities. So far there is limited
89 literature in comparing the soil moisture accuracy of different LSMs options in the WRF model.
90 Therefore, in this study, we select three of the WRF's most advanced LSM schemes (i.e., Noah,
91 Noah-Multiparameterization (Noah-MP), and CLM4) to compare their soil moisture performance
92 for landslide hazard assessment. Furthermore, since all the three schemes can provide multi-layer
93 soil moisture information, it is useful to include all those simulations for the comparison so that

94 the optimal depth of soil moisture could be determined for the landslide monitoring application.
95 In order to compare with the performance of our previous study on using the satellite soil moisture
96 data (Zhuo et al., 2019), the same study area called Emilia Romagna is used here. The study period
97 covers 10 years from 2006 to 2015 to include a long-term record of landslide events. In addition,
98 because slope angle is one of the major factors controlling the stability of the slope, it is hence
99 used in this study to divide the study area into several slope groups, so that a more accurate
100 landslide prediction model could be built.

101 The description of the study area and the used datasets are included in Section 2. Methodologies
102 regarding the WRF model, the related LSM schemes and the adopted landslide threshold
103 evaluation approach are provided in Section 3. Section 4 shows the WRF soil moisture evaluation
104 results against the in-situ observations, and the WRF rainfall evaluations over the whole study area.
105 Section 5 covers the comparison results of the WRF modelled soil moisture products for landslide
106 applications. The discussions and conclusions of the study are included in Section 6 and 7,
107 respectively.

108 ## 2. Study Area and Datasets

109 ### 2.1 Study Area

110 The study area is in the Emilia Romagna Region, northern Italy (Figure 1). Its population density
111 is high. The region has high mountainous areas in the S-SW, and wide plain areas towards NE,
112 with a large elevation difference (i.e., 0 m to 2125 m) across 50 km distance from the north to the
113 south (Rossi et al., 2010). The region has a mild Mediterranean climate with distinct wet and dry
114 seasons (i.e., dry season between May and October, and wet season between November and April).
115 The study area tends to be affected by landslide events easily, with approximately one-fifth of the

mountainous zone covered by active or dormant landslide deposits (Bertolini et al., 2005). Rainfall is by far the primary triggering factor of landslides in the region, followed by snow melting: shallow landslides are mainly triggered by short but exceptionally intense rainfall, and long and moderate rainfall events over saturated conditions, while deep-seated landslides have a more complex response to rainfall and are mainly caused by moderate but exceptionally prolonged (even up to 6 months) periods of rainfalls (Segoni et al., 2015). Due to the abundant data available in the region, several studies on regional scale landslide prediction and early warning have been published (Berti et al., 2012;Martelloni et al., 2012;Lagomarsino et al., 2015;Segoni et al., 2018b;Segoni et al., 2018a;Lagomarsino et al., 2013). Interested readers can refer to those studies for more information.

### 2.2 Selection of The Landslide Events

The landslides catalog is collected from the Emilia Romagna Geological Survey (Berti et al., 2012). The information included in the catalog are: location, date of occurrence, the uncertainty of date, landslide characteristics (dimensions, type, and material), triggering factors, damages, casualties, and references. Unfortunately, many pieces of the information are missing from the records in many cases. In order to organise the data in a more systematic way so that only the relevant events are retained, a two-step event selection procedure is initially carried out based on: 1) rainfall-induced only; and 2) high spatial-temporal accuracy (exact date and coordinates). Finally, a revision of the information about the type of slope instabilities such as landslide/debris flow/rockfall and the characteristics of the affected slope (natural or artificial) is also carried out over the selected records (Valenzuela et al., 2018). The catalog period used in this study covers between 2006 and 2015, which is in accordance with the WRF model run. After filtering the data records, only one-fifth of them (i.e., 157 events) is retained. The retained events are shown as

single circles in Figure 2, with slope information (calculated through the Digital Elevation Model (DEM) data) also presented in the background. It can be seen the spatial distribution of the occurred landslide events is very heterogeneous, with nearly all of them occurred in the hilly regions.

### 2.3 Datasets

There is a total of 19 soil moisture stations available within the study area, however, based on our collected data, only one of them at the San Pietro Capofiume (latitude 44° 39' 13.59", longitude 11° 37' 21.6") provides long-term valid soil moisture retrievals (i.e., 2006 to 2017). We have checked the data from all the rest of the stations, they are either absent (or have very big data gaps) or do not cover the research period at all. Therefore, only the San Pietro Capofiume station is used for the WRF soil moisture temporal evaluation. The soil moisture is measured from 10 cm to 180 cm deep in the soil at 5 depths, by the Time Domain Reflectometry (TDR) instrument. Data are recorded in the unit of volumetric water content ($m^3/m^3$) and at daily timestep (Pistocchi et al., 2008). The data used in this study is between 2006 and 2015. Rainfall data over the whole study area is collected from over 200 tipping-bucket rain gauges, which are used to assess the quality of the WRF model's rainfall estimations in the study area, as well as for rainfall events selection during the Year 2014 and 2015.

To drive a NWP model like WRF for soil moisture simulations, several globally-coved data products can be chosen for extracting the boundary and initial conditions information, for instance, the European Centre for Medium-Range Weather Forecasts (ECMWF) reanalysis (ERA-Interim) and the National Centre for Environmental Prediction (NCEP) reanalysis are two of the most commonly used data products. It has been found by (Srivastava et al., 2013b) that the ERA-Interim datasets can provide better boundary conditions than the NCEP datasets for WRF hydro-

meteorological predictions in Europe, which is therefore adopted in this study to drive the WRF model. The spatial resolution of the ERA-Interim is approximately 80 km. The data is available from 1979 to present, containing 6-hourly gridded estimates of three-dimensional meteorological variables, and 3-hourly estimates of a large number of surface parameters and other two-dimensional fields. A comprehensive description of the ERA-Interim datasets can be found in (Dee et al., 2011)

The Shuttle Radar Topography Mission (SRTM) 3 Arc-Second Global (~ 90m) DEM datasets are downloaded and used as the basis for the slope degree calculations. SRTM DEM data has been widely used for elevation-related studies worldwide due to its high quality, near-global coverage, and free availability (Berry et al., 2007).

## 3. Methodologies

### 3.1 WRF Model and The Three Land Surface Model Schemes

The WRF model is a next-generation, non-hydrostatic mesoscale NWP system designed for both atmospheric research and operational forecasting applications (Skamarock et al., 2005). The model is powerful enough in modelling a broad range of meteorological applications varying from tens of metres to thousands of kilometres (NCAR, 2018). It has two dynamical solvers: the ARW (Advanced Research WRF) core and the NMM (Nonhydrostatic Mesoscale Model) core. The former has more complex dynamic and physics settings than the latter which only has limited setting choices. Hence in this study WRF with ARW dynamic core (version 3.8) is used to perform all the soil moisture simulations.

The main task of LSM within the WRF is to integrate information generated through the surface layer scheme, the radiative forcing from the radiation scheme, the precipitation forcing from the

184 microphysics and convective schemes, and the land surface conditions to simulate the water and
185 energy fluxes (Ek et al., 2003). WRF provides several LSM options, among which three of them
186 are selected in this study as mentioned in the introduction: Noah, Noah-MP, and CLM4. Table 1
187 gives a simple comparison of the three models. The detailed description of the models is written
188 below in the order of increasing complexity in regards of the way they deal with thermal and
189 moisture fluxes in various layers of soil, and their vegetation, root and canopy effects
190 (Skamarock et al., 2008).

191 **3.1.1 Noah**

192 Noah is the most basic amongst the three selected LSMs. It is one of the 'second generation' LSMs
193 that relies on both soil and vegetation processes for water budgets and surface energy closures
194 (Wei et al., 2010). The model is capable of modelling soil and land surface temperature, snow
195 water equivalent, as well as the general water and energy fluxes. The model includes four soil
196 layers that reach a total depth of 2 m in which soil moisture is calculated. Its bulk layer of canopy
197 -snow-soil (i.e., lack the abilities in simulating photosynthetically active radiation (PAR),
198 vegetation temperature, correlated energy, and water, heat and carbon fluxes), 'leaky' bottom (i.e.,
199 drained water is removed immediately from the bottom of the soil column which can result in
200 much fewer memories of antecedent weather and climate fluctuations) and simple snow melt-thaw
201 dynamics are seen as the model's demerits (Wharton et al., 2013). Noah calculates the soil moisture
202 from the diffusive form of Richard's equation for each of the soil layer (Greve et al., 2013), and
203 the evapotranspiration from the Ball-Berry equation (considering both the water flow mechanism
204 within soil column and vegetation, as well as the physiology of photosynthesis (Wharton et al.,
205 2013)).

206 **3.1.2 Noah-MP**

Noah-MP (Niu et al., 2011) is an improved version of the Noah LSM, in the aspect of better representations of terrestrial biophysical and hydrological processes. Major physical mechanism improvements directly relevant to soil water simulations include: 1) introducing a more permeable frozen soil by separating permeable and impermeable fractions (Cai, 2015), 2) adding an unconfined aquifer immediately beneath the bottom of the soil column to allow the exchange of water between them (Liang et al., 2003), and 3) the adoption of a TOPMODEL (TOPography based hydrological MODEL)-based runoff scheme (Niu et al., 2005) and a simple SIMGM groundwater model (Niu et al., 2007) which are both important in improving the modelling of soil hydrology. Noah-MP is unique compared with the other LSMs, as it is capable of generating thousands of parameterisation schemes through the different combinations of "dynamic leaf, canopy stomatal resistance, runoff and groundwater, a soil moisture factor controlling stomatal resistance (the β factor), and six other processes" (Cai, 2015). The scheme option used in the study are: Ball-Berry scheme for canopy stomatal resistance, Monin-Obukhov scheme for surface layer drag coefficient calculation, the Noah based soil moisture factor for stomatal resistance, the TOPMODEL runoff with the SIMGM groundwater, the linear effect scheme for soil permeability, the two-stream applied to vegetated fraction scheme for radiative transfer, the CLASS (Canadian Land Surface Scheme) scheme for ground surface albedo option, and the Jordan (Jordan, 1991) scheme for partitioning precipitation between snow and rain.

### 3.1.3. CLM4

CLM4 is developed by the National Center for Atmospheric Research (NCAR) to serve as the land component of its Community Earth System Model (formerly known as the Community Climate System Model) (Lawrence et al., 2012). It is a 'third generation' model that incorporates the interactions of both nitrogen and carbon in the calculations of water and energy fluxes. Compared

with its previous versions, CLM4 (Oleson et al., 2008) has multiple enhancements relevant to soil moisture computing. For instance, the model's soil moisture is estimated by adopting an improved one-dimensional Richards equation (Zeng and Decker, 2009); the new version allows the dynamic interchanges of soil water and groundwater through an improved definition of the soil column's lower boundary condition that is similar to the Noah-MP's (Niu et al., 2007). Furthermore, the thermal and hydrologic properties of organic soil are included for the modelling which is based on the method developed in (Lawrence and Slater, 2008). The total ground column is extended to 42 m depth, consisting 10 soil layers unevenly spaced between the top layer (0.0–1.8 cm) and the bottom layers (229.6–380.2 cm), and 5 bedrock layers to the bottom of the ground column (Lawrence et al., 2011). Soil moisture is estimated for each soil layer.

### 3.2 WRF Model Parameterization

The WRF model is centred over the Emilia Romagna Region with three nested domains (D1, D2, D3 with the horizontal grid sizes of 45 km, 15 km, and 5 km, respectively), of which the innermost domain (D3, with 88 x 52 grids (west-east and south-north, respectively)) is used in this study. A two-way nesting scheme is adopted allowing information from the child domain to be fed back to the parent domain. With atmospheric forcing, static inputs (e.g., soil and vegetation types), and parameters, the WRF model needs to be spin-up to reach its equilibrium state before it can be used (Cai et al., 2014;Cai, 2015). In this study, WRF is spin-up by running through the whole year of 2005. After the spin-up, the WRF model for each of the selected LSM scheme is executed in daily timestep from January 1, 2006, to December 31, 2015, using the ERA-Interim datasets.

The microphysics scheme plays a vital role in simulating accurate rainfall information which in turn is important for modelling the accurate soil moisture variations. WRF V3.8 is supporting 23 microphysics options range from simple to more sophisticated mixed-phase physical options. In

this study, the WRF Single-Moment 6-class scheme is adopted which considers ice, snow and graupel processes and is suitable for high-resolution applications (Zaidi and Gisen, 2018). The physical options used in the WRF setup are Dudhia shortwave radiation (Dudhia, 1989) and Rapid Radiative Transfer Model (RRTM) longwave radiation (Mlawer et al., 1997). Cumulus parameterization is based on the Kain-Fritsch scheme (Kain, 2004) which is capable of representing sub-grid scale features of the updraft and rain processes, and such a capability is beneficial for real-time modelling (Gilliland and Rowe, 2007). The surface layer parameterization is based on the Revised fifth-generation Pennsylvania State University–National Center for Atmospheric Research Mesoscale Model (MM5) Monin-Obukhov scheme (Jiménez et al., 2012). The Yonsei University scheme (Hong et al., 2006) is selected to calculate the planetary boundary layer. The parameterization schemes used in the WRF modelling are shown in Table 2. The datasets for land use and soil texture are available in the pre-processing package of WRF. In this study, the land use categorisation is interpolated from the MODIS 21-category data classified by the International Geosphere Biosphere Programme (IGBP). The soil texture data are based on the Food and Agriculture Organization of the United Nations Global 5-minutes soil database.

### 3.3 Translation of Observed and Simulated Soil Moisture Data to Common Soil Layers

Since all soil moisture datasets have different soil depths, it is difficult for a direct comparison. The Noah and Noah-MP models include four soil layers, centred at 5, 25, 70, and 150 cm, respectively. Whereas CLM4 model has 10 soil layers, centered at 0.9, 3.2, 6.85, 12.85, 22.8, 39.2, 66.2, 110.65, 183.95, 304.9 cm, respectively. Moreover, the in-situ sensor measures soil moisture centred at 10, 25, 70, 135, and 180 cm. In order to make the datasets comparable at consistent soil depths, the simple linear interpolation approach described in (Zhuo et al., 2015b) is applied in this study, and a benchmark of the soil layer centred at 10, 25, 70 and 150 cm is adopted.

### 3.4 Soil Moisture Thresholds Build Up and Evaluations

To build and evaluate the soil moisture thresholds for landslides forecasting, all datasets have been grouped into two portions: 2006-2013 for the establishment of thresholds, and 2014-2015 for the evaluation. The determination of soil moisture thresholds is based on determining the most suitable soil moisture triggering level for landslides occurrence by trying a range of exceedance probabilities (percentiles). For example, a 10% exceedance probability is calculated by determining the 10% percentile result of the soil moisture datasets that are related to the occurred landslides. The exceedance probability method is commonly utilised in landslide early warning studies for calculating the rainfall-thresholds, which is therefore adopted here to examine its performance for soil moisture threshold calculations.

To carry out the threshold evaluation, 45 rainfall events (during 2014-2015) are selected for the purpose. The rainfall events are separated based on at least one-day of dry period (i.e., a period without rainfall). The rainfall data from each rain gauge station is firstly combined using the Thiessen Polygon method, and with visual analysis, the 45 events are then finally selected. The information about the selected rainfall events can be found in Section 5. The threshold evaluation is based on the statistical approach described in (Gariano et al., 2015;Zhuo et al., 2019), where soil moisture threshold can be treated as a binary classifier of the soil moisture conditions that are likely or unlikely to cause landslide events. With this hypothesis, the likelihood of a landslide event can either be *true* (*T*) or *false* (*F*), and the threshold forecasting can either be *positive* (*P*) or *negative* (*N*). The combinations of those four conditions can lead to four statistical outcomes (Figure 3a) that are: *true positive* (*TP*), *true negative* (*TN*), *false positive* (*FP*), and *false negative* (*FN*) (Wilks, 2011). Using the four outcomes, two statistical scores can be determined.

The Hit Rate (*HR*), which is the rate of the events that are correctly forecasted. Its formula is:

$$HR = \frac{TP}{TP+FN} \quad (1)$$

in the range of 0 and 1, with the best result as 1.

The False Alarm Rate *(FAR*), which is the rate of false alarms when the event did not occur. Its formula is:

$$FAR = \frac{FP}{FP+TN} \quad (2)$$

in the range of 0 and 1, with the best result as 0.

For any soil moisture product, each threshold calculated is adopted to determine *T*, *F*, *P*, and *N*, respectively. Those values are finally integrated to find the overall scores of *TP*, *FN*, *FP*, *TN*, *HR*, and *FAR*. The threshold performance is then judged via the Receiver Operating Characteristic (ROC) analysis (Hosmer and Lemeshow, 1989;Fawcett, 2006). As shown in Figure 3b, ROC curve is based on *HR* against *FAR*, and each point in the curve represents a threshold scenario (i.e., selected exceedance probabilities). The optimal result (the red point) can only be realised when the *HR* reaches 1 and the *FAR* reduces to 0. The closer the point to the red point, the better the forecasting result is. To analyse and compare the forecasting performance numerically, the Euclidean distances (*d*) for each scenario to the optimal point are computed.

## 4. WRF Model Evaluations

In this study, the evaluation is based on the daily mean soil moisture. The reason for not using the antecedent soil moisture condition plus rainfall data on the day is because the purpose of this study is to explore the relationship between different WRF simulated soil moisture and landslides solely. In general, soil moisture is a predisposing factor for slope instability, while rainfall is the triggering factor. The same rainfall may trigger or not a landslide depending on the soil moisture content at the time of the rainfall event. The mean soil moisture on the day of the landslide implicitly account for both the initial soil moisture and the effective rainfall absorbed by the ground, and can be a robust indicator of the hydrological condition of the slope.

### 4.1 Soil Moisture Temporal Comparisons

Although there is only one soil moisture sensor that provides long-term soil moisture data in the study region, it is still useful to compare it with the WRF estimated soil moisture. In this study, we carry out a temporal comparison between all the three WRF soil moisture products with the in-situ observations (at a single soil moisture measuring point in the plain area). The comparison is implemented over the period from 2006 to 2015, and the WRF grid closest to the in-situ sensor location is chosen. Figure 4 shows the comparison results at the four soil depths. The statistical performance (correlation coefficient *r* and Root Mean Square Error *RMSE*) of the three LSM schemes are summarised in Table 3. Based on the statistical results, Noah-MP surpasses other schemes at most soil layers, except for Layer 2 where CLM4 shows stronger correlation and Layer 4 where Noah gives smaller *RMSE* error. For Noah-MP, the best correlation is observed at the surface layer (0.809), followed by the third (0.738), second (0.683) and fourth (0.498) layers; and based on *RMSE,* the best performance is again observed at the surface layer and followed by the second, third and fourth layers in sequence (as 0.060, 0.070, 0.088, and 0.092 $m^3/m^3$, respectively). From the temporal plots, it can be seen at all four soil layers, all three LSM schemes can produce the soil moisture's seasonal cycle with most upward and downward trends successfully represented. However, both the Noah and the CLM4 overestimate the variability at the upper two soil layers during almost the whole study period, and the situation is the worst for the Noah. Comparatively, the Noah-MP can better capture the wet soil moisture conditions especially at the surface layer; and it is the only model of the three that is able to simulate the large soil drying phenomenon close to the observations during the dry season, except for some extremely dry days. Towards 70 cm depth, although Noah-MP is still able to capture most of the soil moisture variabilities during the drying period, it significantly underestimates soil moisture values for most wet days. Similar

346 underestimation results can be observed for CLM4 and Noah during the wet season at 70 cm;
347 furthermore, both schemes are again not capable of reproducing the extremely drying phenomenon
348 and overestimate soil moisture for most of the dry season days. It is surprising to see that at the
349 deep soil layer (150 cm), all soil moisture products are underestimated, in particular, the outputs
350 from the CLM4 and the Noah-MP only show small fluctuations. However, the soil moisture
351 measurements from the in-situ sensor also get our attention as they show strange fluctuations with
352 numerous sudden drops and rise situations observed. The strange phenomenon is not expected at
353 such a deep soil layer (although groundwater capillary forces can increase the soil moisture, its
354 rate is normally very slow). One possible reason we suspect is due to sensor failure in the deep
355 zone. Therefore, the assessment result for the deep soil layer should be considered unreliable.
356 Overall for the Noah-MP, in addition to producing the highest correlation coefficient and the
357 lowest *RMSE*, its simulated soil moisture variations are the closest to the observations. The better
358 performance of the Noah-MP over the other two models agrees with the results found in (Cai et
359 al., 2014) (note: the paper uses standalone models, which are not coupled with WRF). Also, it has
360 been discussed in (Yang et al., 2011), the Noah MP presents a clear improvement over the Noah
361 in simulating soil moisture globally. However, it is noted the evaluation results are only based on
362 one soil moisture sensor located at the plain part of the study area.

363 **4.2 Rainfall Evaluations**

364 Since soil moisture is related to rainfall, it is useful to carry out the evaluations of WRF rainfall
365 estimations against the observations in the study area. The spatial plot of *R* for the three LSMs is
366 shown in Figure 5. It can be seen the performance of the three models are very close to each other,
367 with only small differences over the whole study region. In general, the performance is the best in
368 the Southeast region, with *R* reaches above 0.70. The poorest performance is observed in the

Northeast region and some parts of the mountain zone. Based on the spatial distribution of *R*, there is no clear correlation between the WRF rainfall performance and the topography of the region. The boxplot for the *R* performance is illustrated in Figure 6a. It can be seen again the performances of the three models are very similar. Generally, *R* ranges between around 0.10 and 0.80, and with the majority of the region performs around 0.40. *RMSE* performance is also calculated. Similar to the results of *R*, it has been found the *RMSE* spatial distributions are very similar among the three models. Therefore, the *RMSE* spatial distribution map is not included in this paper. The boxplot of the *RMSE* is shown in Figure 6b. Generally, the *RMSE* ranges between around 4 mm and 12 mm, with some outliers between around 12 mm and 20 mm. Majority of the region performs at around 7 mm *RMSE*. The statistical calculations are summarised in Table 4. Based on the results of *R* and *RMSE*, the WRF rainfall estimation performance in Emilia is similar to the one found in central USA (Van Den Broeke et al., 2018).

## 5. The Assessment of WRF Soil Moisture Threshold for Landslide Monitoring

As introduced at the beginning of the paper, previous works (as discussed in the introduction section) have demonstrated that in complex geomorphologic settings (e.g., in Emilia Romagna), a rainfall threshold approach is too simple and more hydrologically driven approaches need to be established. This section is to assess if the spatial distribution of soil moisture can provide useful information for landslide monitoring at the regional scale. Particularly, all three soil moisture products simulated through the WRF model are used to derive threshold models, and the corresponding landslide prediction performances are then compared statistically. Here the threshold is defined as the crucial soil moisture condition above which landslides are likely to happen.

391 Among different factors for controlling the stability of slope, the slope angle is one of the most
392 critical ones. From the slope angle map in Figure 2, it can be seen the region has a clear spatial
393 pattern of high and low slope areas, with the majority of the high-slope areas (can be as steep as
394 around 40 degrees) located in the mountainous Southern part and the river valleys. Based on the
395 analysed events data, the landslides happened during the study period are mainly located in the
396 high-slope region, with a particularly high concentration around the central Southern part. The
397 spatial distribution of the landslide events is also in line with the overall geological characteristics
398 of the region, i.e., the Southern part mainly constitutes outcrop of sandstone rocks that make up
399 the steep slopes and are covered by a thin layer of permeable sandy soil, which are highly unstable.
400 Therefore, instead of only using one soil moisture threshold for the whole study area, it is useful
401 to divide the region into several slope groups so that within each group a threshold model is built.
402 To derive soil moisture threshold individually under different slope conditions, all data has been
403 divided into three groups based on the slope angle (0.4-1.86$^{o}$; 1.87-9.61$^{o}$; 9.52-40.43$^{o}$; since no
404 landslide events are recorded under the 0-0.39$^{o}$ group, the group is not considered here), as results,
405 all groups have equal coverage areas. There are different ways to group the slopes. In this study,
406 in order to have equal coverage areas, we have identified these class-break values.

407 In order to find the optimal threshold so that there are least missing alarms (i.e., threshold is
408 overestimated) and false alarms (i.e., threshold is underestimated), we test out 17 different
409 exceedance probabilities from 1% to 50%. For each LSM scheme, the total number of threshold
410 models is 204, which is the resultant of different combinations of slope groups, soil layers, and
411 exceedance probability conditions. The calculated thresholds for all LSM schemes under three
412 slope groups are plotted in Figure 7. Overall there is a clear trend between the slope angle and the
413 soil moisture threshold, that is with threshold becoming smaller for steeper areas. The correlation

414 is more evident at the upper three soil layers (i.e., the top 1 m depth of soil), with only a few
415 exceptions for Noah and CLM4 at the 1% and the 2% exceedance probabilities. At the deep soil
416 layer centred at 150 cm, the soil moisture threshold difference between Slope Group (S.G.) 2 and
417 3 becomes very small for all the three LSM schemes. This could be partially because at the deep
418 soil layer, the change of soil moisture is much smaller than at the surface layer, therefore the soil
419 moisture values for S.G. 2 and 3 could be too similar to differentiate. However, for milder slopes
420 (S.G. 1), the higher soil moisture triggering level always applies even down to the deepest soil
421 layer for all the three LSM schemes. In this study, the results show that wetter soil can trigger
422 landslides easier in milder slopes than in steeper slopes.

423 All the threshold models are then evaluated under the 45 selected rainfall events (Table 5) using
424 the ROC analysis. Each threshold determined for each of the slope class during the calibration is
425 used for the evaluation. The period of the selected rainfall events is between 1 day and 18 days,
426 and the average rainfall intensity ranges from 5.05 mm/day to 24.69 mm/day. The resultant
427 Euclidean distances (*d*) between each scenario of exceedance probability and the optimal point for
428 ROC analysis are listed in Table 6 for all three WRF LSM schemes at the tested exceedance
429 probabilities. The best performance (i.e., lowest *d*) in each column (i.e., each soil layer of an LSM
430 scheme) is highlighted. In addition, the *d* results are also plotted in Figure 8 to give a better view
431 of the overall trend amongst different soil layers and LSM schemes. From the figure, for all three
432 LSM schemes at all four soil layers, there is an overall downward and then stabilised trend. Overall
433 for Noah, the simulated surface layer soil moisture provides better landslide monitoring
434 performance than the rest of the soil layers from 1% to 35% exceedance probabilities; and the
435 scheme's worst performance is observed at the third soil layer centred at 70 cm. The values of *d*
436 for Noah's second and fourth layer are quite close to each other. For Noah-MP, the simulated

surface layer soil moisture gives the best performance amongst all four soil layers for most cases between the 1% and 35% exceedance probability range; and the scheme's worst performance is observed at the fourth layer. Unlike Noah, all four soil layers from the Noah-MP scheme provide distinct performance amongst them (i.e., larger *d* difference). For CLM4, the performance for the surface layer is quite similar to the second layer's, and the differences between the four layers are small. From the Table 6, it can be seen for Noah the most suitable exceedance probabilities (i.e., the highlighted numbers) range between 35% to 50%; for Noah-MP they are between 30% and 50%, and for CLM4 it stays at 40% for all four soil layers. For both Noah and Noah-MP, the best performance is observed at the surface layer ($d$ = 0.392 and $d$ = 0.369, respectively). For CLM4, the best performances show no distinct pattern amongst soil layers (i.e., with the best performance found at the soil Layer 3, followed by Layer 2, 1, and 4). Of all the LSM schemes and soil layers, the best performance is found for Noah-MP at the surface layer with 30% exceedance probability ($d$=0.369). Based on the *d* results, WRF modelled soil moisture provides better landslide prediction performance than the satellite ESA-CCI soil moisture products as shown in our previous study ((Zhuo et al., 2019), i.e., $d$ = 0.51). The ROC curve for the Noah-MP scheme at the surface layer is shown in Figure 9. In the curve, each point represents a scenario with a selected exceedance probability level. It is clear with various exceedance probabilities, *FAR* can be decreased without sacrificing the *HR* score (e.g., 4% to 10% exceedance probabilities). At the optimal point at the 30% exceedance probability, the best results for *HR* and *FAR* are observed as 0.769 and 0.289, respectively.

## 6. Discussions

In this study, the best landslide prediction performance for Noah and Noah-MP follows a regular trend, that is the deeper the soil layer, the poorer the landslide monitoring performance. There are

several potential reasons for such an outcome. First, the simulated soil moisture accuracy at the shallower layers are better than the deeper zones. Second, although the wetness conditions at the sliding surface are important, the soil moisture above it is also important (i.e., the loading should be heavier with more water in the upper soil layer). Third, the landslides occurred in the region are mainly in the top shallow soil layer. Fourth, the WRF modelled soil moisture is not accurate enough in assessing the landslide events in the study region. In order to find out the extract reasons, comprehensive studies with more detailed landslide events datasets are needed in future studies.

For the WRF soil moisture evaluation, clearly the evaluation work based on a single soil moisture sensor located in plain area is not sufficient to derive conclusions about the model's performance over the whole study region. Therefore, the results are preliminary here. However, in this study, by introducing the WRF spatial soil moisture information into the landslide prediction model, the performance indeed has been improved in comparison with our previous study using the satellite remote sensing soil moisture data (Zhuo et. al 2019). A similar concept has been carried out by Segoni et al., (2018b), who implemented the soil moisture information simulated from a hydrological model into a regional landslide early warning system with clear improvements in false/ missing alarm performance. Although the results shown in this study is preliminary and confined by the study area, the improved landslide prediction performance is already obtained. Therefore, it is hoped with more densely soil moisture network data available globally and further refinements of the method, the results could be improved further.

In addition, ideally, it will be useful if there is a dense soil moisture sensing network covering the whole study area. In reality, that's not practical, so we have to rely on the spatial soil moisture information by other means. So far, the soil moisture data with the best spatial and temporal resolution is from the WRF model. A question is about how representative of a single soil moisture

sensor is for the whole study area. We have carried out the correlation study of a single sensor with the whole study region (using the Noah-MP top-layer soil moisture data). As seen in Figure 10a, the study region is divided into 44 equal-spacing grids (30 km apart), with the grid centres marked as black crosses. The initial assumption is that the soil moisture sensor can only represent its adjacent area, but the result was a surprise (Figure 10b). Based on the outcome, a single point sensor can represent a significant proportion of the region. Admittedly, there are some areas where the correlations are poor, in particular, the Grid 27, which has been compared with its surrounding four grids as shown in Figure 11. It can be seen the soil moisture variation at Grid 27 is totally different in comparison with the four surrounding grids'. The unique soil moisture variation pattern observed in Grid 27 may be caused by different land use and soil type in that area, but clearly further studies are needed to find out the exact reasons. The aforementioned work has prompt us to a future study on the optimal soil moisture sensor network design for landside applications. Although there are numerous studies on the rain gauge network design by the research community, the soil moisture sensor network design has been largely ignored by the community. Hence, this study has paved a foundation for such research.

For the WRF rainfall evaluations, the results are not good. Rainfall is one of the main drivers of soil moisture change, and it is logical to think soil moisture and rainfall are highly linked, However, since rainfall temporal vaiation is of high frequency data while soil moisture is of low frequency, they behave differently. The results illustrate that for landslide study, it is better to use the WRF soil moisture data than its rainfall data. Clearly more studies are needed to confirm this assumption.

Here, WRF is modelled based on the ERA-Interim datasets, however, it has been found in Albergel et al. (2018), the performance of using the ERA5 has surpassed the ERA-Interim. Therefore, the ERA5 datasets will be tested in our future studies. Model-based soil moisture estimations could be

affected by error accumulation issues, especially in the real-time forecasting mode. A potential solution is to use data assimilation methodologies to correct such errors by assimilating soil moisture information from other data sources. Since in-situ soil moisture sensors are only sparsely available in limited regions, soil moisture measured via satellite remote sensing technologies could provide useful alternatives. Another issue is with the landslide record data, since most of them are based on human experiences (e.g., through newspapers, and victims), a lot of incidences could be unreported. Therefore, the conclusion made here could be biased. Other ways of expanding the current landslide catalog can depend on automatic landslide detection methods based on remote sensing images (Nichol and Wong, 2005;Chen et al., 2018), internet news (as all landslides with a relevant impact on society will be reported on internet news), and automatic web data mining methods (Battistini et al., 2013;Goswami et al., 2018).

## 7. Conclusions

In this study, the usability of WRF modelled soil moisture for landslide monitoring has been evaluated in the Emilia Romagna region based on the research duration between 2006 and 2015. Specifically, the four-layer soil moisture information simulated through the WRF's three most advanced LSM schemes (i.e., Noah, Noah-MP and CLM4) is compared for the purpose. Through the temporal comparison with the in-situ soil moisture observations, it has been found that all three LSM schemes at all four soil layers can produce the general soil moisture's seasonal cycle. However, only Noah-MP is able to simulate the large soil drying phenomenon close to the observations during the drying season, and it also has the highest correlation coefficient and the lowest *RMSE* at most soil layers amongst the three LSM schemes. However, it should be noted, the soil moisture evaluation is only based on a single point-based soil moisture sensor that is available in the plain region of the study area. Therefore, the WRF soil moisture performance over

the whole study region, in particular, at the mountainous zone cannot be evaluated in this study. Since soil moisture is related to rainfall, we have carried out the WRF rainfall assessments, based on the comparison with the dense rainfall network in the region. The results have shown that there is no distinct difference between the three LSM schemes. The WRF rainfall performance is found to be similar to a study carried out over the central USA (Van Den Broeke et al., 2018). A landslide prediction model based on soil moisture and slope angle condition is built up. 17 various exceedance probably levels between 1% and 50% are adopted to find the optimal threshold scenario. Through the ROC analysis of 612 threshold models, the best performance is obtained by the Noah-MP at the surface soil layer with 30% exceedance probability.

In summary, this study provides an overview of the soil moisture performance of three WRF LSM schemes for landslide hazard assessment. Based on the results, we demonstrate that the surface soil moisture (centred at 10 cm) simulated through the Noah-MP LSM scheme is useful in predicting landslide occurrences in the Emelia Romagna region. With the hitting rate of 0.769 and the false alarm rate of 0.289 obtained in this study, such soil moisture information has the potential in working with rainfall data to provide landslide predictions. The further study on investigating the soil moisture representation of a single soil moisture sensor over a large region has also been carried out. The results demonstrate that although there is a significant elevation difference in the region, a single soil moisture sensor has a high correlation with a significant proportion of the study area. Although there are still a small proportion of areas where the correlation is poor, this has prompt us to carry out a future study on the optimal design of soil moisture sensor network for landslide study.

One must bear in mind that although the results demonstrated in this study are only valid for the selected region, the methodology could be generalised to derive site-specific calibrations in other

552 sites using the proposed approach. In order to make a general conclusion, more researches are
553 needed using the methodology described in this paper. Particularly, a considerable number of
554 catchments with a broad spectrum of climate and environmental conditions and dense soil moisture
555 sensor network will need to be investigated.

556 **Acknowledgement**

557 This study is supported by Resilient Economy and Society by Integrated SysTems modelling
558 (RESIST), Newton Fund via Natural Environment Research Council (NERC) and Economic and
559 Social Research Council (ESRC) (NE/N012143/1), and the National Natural Science Foundation
560 of China (No：4151101234). The Landslide inventory data is kindly provided by Dr Matteo Berti,
561 University of Bologna.

562 **References**

563 Albergel, C., Dutra, E., Munier, S., Calvet, J.-C., Munoz-Sabater, J., Rosnay, P. d., Balsamo, G. J.
564 H., and Sciences, E. S.: ERA-5 and ERA-Interim driven ISBA land surface model simulations:
565 which one performs better?, 22, 3515-3532, 2018.

566 Battistini, A., Segoni, S., Manzo, G., Catani, F., and Casagli, N. J. A. G.: Web data mining for
567 automatic inventory of geohazards at national scale, 43, 147-158, 2013.

568 Berry, P., Garlick, J., and Smith, R.: Near-global validation of the SRTM DEM using satellite
569 radar altimetry, Remote Sensing of Environment, 106, 17-27, 2007.

570 Berti, M., Martina, M., Franceschini, S., Pignone, S., Simoni, A., and Pizziolo, M.: Probabilistic
571 rainfall thresholds for landslide occurrence using a Bayesian approach, Journal of Geophysical
572 Research: Earth Surface, 117, 2012.

573 Bertolini, G., Guida, M., and Pizziolo, M. J. L.: Landslides in Emilia-Romagna region (Italy):
574 strategies for hazard assessment and risk management, 2, 302-312, 2005.

Bittelli, M., Valentino, R., Salvatorelli, F., and Pisa, P. R.: Monitoring soil-water and displacement conditions leading to landslide occurrence in partially saturated clays, Geomorphology, 173, 161-173, 2012.

Bogaard, T., and Greco, R.: Invited perspectives: Hydrological perspectives on precipitation intensity-duration thresholds for landslide initiation: proposing hydro-meteorological thresholds, Natural Hazards and Earth System Sciences, 18, 31-39, 2018.

Cai, X., Yang, Z. L., Xia, Y., Huang, M., Wei, H., Leung, L. R., and Ek, M. B.: Assessment of simulated water balance from Noah, Noah-MP, CLM, and VIC over CONUS using the NLDAS test bed, Journal of Geophysical Research: Atmospheres, 119, 13,751-713,770, 2014.

Cai, X.: Hydrological assessment and biogeochemical advancement of the Noah-MP land surface model, Doctor of Philosophy, Geological Sciences, The University of Texas at Austin, 164 pp., 2015.

Chae, B.-G., Park, H.-J., Catani, F., Simoni, A., and Berti, M.: Landslide prediction, monitoring and early warning: a concise review of state-of-the-art, Geosciences Journal, 21, 1033-1070, 2017.

Chen, F., and Dudhia, J.: Coupling an advanced land surface-hydrology model with the Penn State-NCAR MM5 modeling system. Part I: Model implementation and sensitivity, Monthly Weather Review, 129, 569-585, 2001.

Chen, Z., Zhang, Y., Ouyang, C., Zhang, F., and Ma, J. J. S.: Automated landslides detection for mountain cities using multi-temporal remote sensing imagery, 18, 821, 2018.

Ciabatta, L., Camici, S., Brocca, L., Ponziani, F., Stelluti, M., Berni, N., and Moramarco, T. J. J. o. H.: Assessing the impact of climate-change scenarios on landslide occurrence in Umbria Region, Italy, 541, 285-295, 2016.

Crozier, M. J.: Prediction of rainfall-triggered landslides: A test of the antecedent water status model, Earth surface processes and landforms, 24, 825-833, 1999.

Dee, D. P., Uppala, S. M., Simmons, A., Berrisford, P., Poli, P., Kobayashi, S., Andrae, U., Balmaseda, M., Balsamo, G., and Bauer, d. P.: The ERA-Interim reanalysis: Configuration and performance of the data assimilation system, Quarterly Journal of the royal meteorological society, 137, 553-597, 2011.

Dorigo, W., Wagner, W., Albergel, C., Albrecht, F., Balsamo, G., Brocca, L., Chung, D., Ertl, M., Forkel, M., and Gruber, A.: ESA CCI Soil Moisture for improved Earth system understanding: State-of-the art and future directions, Remote Sensing of Environment, 203, 185-215, 2017.

Dudhia, J.: Numerical study of convection observed during the winter monsoon experiment using a mesoscale two-dimensional model, Journal of the Atmospheric Sciences, 46, 3077-3107, 1989.

Ek, M., Mitchell, K., Lin, Y., Rogers, E., Grunmann, P., Koren, V., Gayno, G., and Tarpley, J.: Implementation of Noah land surface model advances in the National Centers for Environmental Prediction operational mesoscale Eta model, Journal of Geophysical Research: Atmospheres, 108, 2003.

Fawcett, T.: An introduction to ROC analysis, Pattern recognition letters, 27, 861-874, 2006.

Gao, Q., Zribi, M., Escorihuela, M., and Baghdadi, N. J. S.: Synergetic use of Sentinel-1 and Sentinel-2 data for soil moisture mapping at 100 m resolution, 17, 1966, 2017.

Gariano, S. L., Brunetti, M. T., Iovine, G., Melillo, M., Peruccacci, S., Terranova, O., Vennari, C., and Guzzetti, F.: Calibration and validation of rainfall thresholds for shallow landslide forecasting in Sicily, southern Italy, Geomorphology, 228, 653-665, 2015.

Geudtner, D., Torres, R., Snoeij, P., Davidson, M., and Rommen, B.: Sentinel-1 system capabilities and applications, 2014 IEEE Geoscience and Remote Sensing Symposium, 2014, 1457-1460,

Gilliland, E. K., and Rowe, C. M.: A comparison of cumulus parameterization schemes in the WRF model, Proceedings of the 87th AMS Annual Meeting & 21th Conference on Hydrology, 2007,

Glade, T., Crozier, M., and Smith, P.: Applying probability determination to refine landslide-triggering rainfall thresholds using an empirical "Antecedent Daily Rainfall Model", Pure and Applied Geophysics, 157, 1059-1079, 2000.

Goswami, S., Chakraborty, S., Ghosh, S., Chakrabarti, A., and Chakraborty, B. J. A. S. E. J.: A review on application of data mining techniques to combat natural disasters, 9, 365-378, 2018.

Greve, P., Warrach-Sagi, K., and Wulfmeyer, V.: Evaluating soil water content in a WRF-Noah downscaling experiment, Journal of Applied Meteorology and Climatology, 52, 2312-2327, 2013.

630 Hawke, R., and McConchie, J.: In situ measurement of soil moisture and pore-water pressures in
631 an 'incipient'landslide: Lake Tutira, New Zealand, Journal of environmental management, 92,
632 266-274, 2011.

633 Hong, S.-Y., Noh, Y., and Dudhia, J.: A new vertical diffusion package with an explicit treatment
634 of entrainment processes, Monthly Weather Review, 134, 2318-2341, 2006.

635 Hosmer, D., and Lemeshow, S.: Applied logistic regression. 1989, New York: Johns Wiley & Sons,
636 1989.

637 Jiménez, P. A., Dudhia, J., González-Rouco, J. F., Navarro, J., Montávez, J. P., and García-
638 Bustamante, E.: A revised scheme for the WRF surface layer formulation, Monthly Weather
639 Review, 140, 898-918, 2012.

640 Jordan, R.: A one-dimensional temperature model for a snow cover: Technical documentation for
641 SNTHERM. 89, Cold Regions Research and Engineering Laboratory, 1991.

642 Kain, J. S.: The Kain-Fritsch convective parameterization: An update, Journal of Applied
643 Meteorology, 43, http://dx.doi.org/10.1175/1520-0450(2004)043<0170:TKCPAU>2.0.CO;2,
644 2004.

645 Klose, M., Highland, L., Damm, B., and Terhorst, B.: Estimation of Direct Landslide Costs in
646 Industrialized Countries: Challenges, Concepts, and Case Study, in: Landslide Science for a Safer
647 Geoenvironment, World Landslide Forum 3, China (Beijing), 2014, 661-667,

648 Lagomarsino, D., Segoni, S., Fanti, R., and Catani, F. J. L.: Updating and tuning a regional-scale
649 landslide early warning system, 10, 91-97, 2013.

650 Lagomarsino, D., Segoni, S., Rosi, A., Rossi, G., Battistini, A., Catani, F., Casagli, N. J. N. H.,
651 and Sciences, E. S.: Quantitative comparison between two different methodologies to define
652 rainfall thresholds for landslide forecasting, 15, 2413-2423, 2015.

653 Lawrence, D. M., and Slater, A. G.: Incorporating organic soil into a global climate model, Climate
654 Dynamics, 30, 145-160, 2008.

655 Lawrence, D. M., Oleson, K. W., Flanner, M. G., Thornton, P. E., Swenson, S. C., Lawrence, P.
656 J., Zeng, X., Yang, Z. L., Levis, S., and Sakaguchi, K.: Parameterization improvements and

functional and structural advances in version 4 of the Community Land Model, Journal of Advances in Modeling Earth Systems, 3, 27, 2011.

Lawrence, D. M., Oleson, K. W., Flanner, M. G., Fletcher, C. G., Lawrence, P. J., Levis, S., Swenson, S. C., and Bonan, G. B.: The CCSM4 land simulation, 1850–2005: Assessment of surface climate and new capabilities, Journal of Climate, 25, 2240-2260, 2012.

Leung, L. R., and Qian, Y.: Atmospheric rivers induced heavy precipitation and flooding in the western US simulated by the WRF regional climate model, Geophysical research letters, 36, 2009.

Liang, X., Xie, Z., and Huang, M.: A new parameterization for surface and groundwater interactions and its impact on water budgets with the variable infiltration capacity (VIC) land surface model, Journal of Geophysical Research: Atmospheres, 108, 2003.

Maheu, A., Anctil, F., Gaborit, É., Fortin, V., Nadeau, D. F., and Therrien, R.: A field evaluation of soil moisture modelling with the Soil, Vegetation, and Snow (SVS) land surface model using evapotranspiration observations as forcing data, Journal of Hydrology, 558, 532-545, 2018.

Martelloni, G., Segoni, S., Fanti, R., and Catani, F. J. L.: Rainfall thresholds for the forecasting of landslide occurrence at regional scale, 9, 485-495, 2012.

Mlawer, E. J., Taubman, S. J., Brown, P. D., Iacono, M. J., and Clough, S. A.: Radiative transfer for inhomogeneous atmospheres: RRTM, a validated correlated-k model for the longwave, Journal of Geophysical Research: Atmospheres, 102, 16663-16682, 1997.

Weather research and forcasting model, 2018.

Nichol, J., and Wong, M. J. I. j. o. r. s.: Satellite remote sensing for detailed landslide inventories using change detection and image fusion, 26, 1913-1926, 2005.

Niu, G. Y., Yang, Z. L., Dickinson, R. E., and Gulden, L. E.: A simple TOPMODEL-based runoff parameterization (SIMTOP) for use in global climate models, Journal of Geophysical Research: Atmospheres, 110, 2005.

Niu, G. Y., Yang, Z. L., Dickinson, R. E., Gulden, L. E., and Su, H.: Development of a simple groundwater model for use in climate models and evaluation with Gravity Recovery and Climate Experiment data, Journal of Geophysical Research: Atmospheres, 112, 2007.

Niu, G. Y., Yang, Z. L., Mitchell, K. E., Chen, F., Ek, M. B., Barlage, M., Kumar, A., Manning, K., Niyogi, D., and Rosero, E.: The community Noah land surface model with multiparameterization options (Noah-MP): 1. Model description and evaluation with local-scale measurements, Journal of Geophysical Research: Atmospheres, 116, 2011.

Oleson, K., Niu, G. Y., Yang, Z. L., Lawrence, D., Thornton, P., Lawrence, P., Stöckli, R., Dickinson, R., Bonan, G., and Levis, S.: Improvements to the Community Land Model and their impact on the hydrological cycle, Journal of Geophysical Research: Biogeosciences (2005–2012), 113, 2008.

Oleson, K. W., Lawrence, D. M., Gordon, B., Flanner, M. G., Kluzek, E., Peter, J., Levis, S., Swenson, S. C., Thornton, E., and Feddema, J.: Technical description of version 4.0 of the Community Land Model (CLM), 2010.

Paloscia, S., Pettinato, S., Santi, E., Notarnicola, C., Pasolli, L., and Reppucci, A. J. R. S. o. E.: Soil moisture mapping using Sentinel-1 images: Algorithm and preliminary validation, 134, 234-248, 2013.

Pistocchi, A., Bouraoui, F., and Bittelli, M.: A simplified parameterization of the monthly topsoil water budget, Water Resources Research, 44, 2008.

Ponziani, F., Pandolfo, C., Stelluti, M., Berni, N., Brocca, L., and Moramarco, T. J. L.: Assessment of rainfall thresholds and soil moisture modeling for operational hydrogeological risk prevention in the Umbria region (central Italy), 9, 229-237, 2012.

Posner, A. J., and Georgakakos, K. P.: Soil moisture and precipitation thresholds for real-time landslide prediction in El Salvador, Landslides, 12, 1179-1196, 2015.

Rossi, M., Witt, A., Guzzetti, F., Malamud, B. D., Peruccacci, S. J. E. S. P., and Landforms: Analysis of historical landslide time series in the Emilia-Romagna region, northern Italy, 35, 1123-1137, 2010.

Segoni, S., Lagomarsino, D., Fanti, R., Moretti, S., and Casagli, N.: Integration of rainfall thresholds and susceptibility maps in the Emilia Romagna (Italy) regional-scale landslide warning system, Landslides, 12, 773-785, 2015.

711 Segoni, S., Rosi, A., Fanti, R., Gallucci, A., Monni, A., and Casagli, N. J. W.: A Regional-Scale
712 Landslide Warning System Based on 20 Years of Operational Experience, 10, 1297, 2018a.

713 Segoni, S., Rosi, A., Lagomarsino, D., Fanti, R., and Casagli, N.: Brief communication: Using
714 averaged soil moisture estimates to improve the performances of a regional-scale landslide early
715 warning system, Natural Hazards and Earth System Sciences, 18, 807-812, 2018b.

716 Skamarock, W., Klemp, J., Dudhia, J., Gill, D., Barker, D., Duda, M., Huang, X., Wang, W., and
717 Powers, J.: A description of the advanced research WRF Version 3, NCAR technical note,
718 Mesoscale and Microscale Meteorology Division, National Center for Atmospheric Research,
719 Boulder, Colorado, USA, 2008.

720 Skamarock, W. C., Klemp, J. B., Dudhia, J., Gill, D. O., Barker, D. M., Wang, W., and Powers, J.
721 G.: A description of the advanced research WRF version 2, National Center For Atmospheric
722 Research Boulder Co Mesoscale and Microscale Meteorology Div, 2005.

723 Srivastava, P. K., Han, D., Rico-Ramirez, M. A., Al-Shrafany, D., and Islam, T.: Data fusion
724 techniques for improving soil moisture deficit using SMOS satellite and WRF-NOAH land surface
725 model, Water resources management, 27, 5069-5087, 2013a.

726 Srivastava, P. K., Han, D., Rico Ramirez, M. A., and Islam, T.: Comparative assessment of
727 evapotranspiration derived from NCEP and ECMWF global datasets through Weather Research
728 and Forecasting model, Atmospheric Science Letters, 14, 118-125, 2013b.

729 Srivastava, P. K., Han, D., Rico-Ramirez, M. A., O'Neill, P., Islam, T., Gupta, M., and Dai, Q.:
730 Performance evaluation of WRF-Noah Land surface model estimated soil moisture for
731 hydrological application: Synergistic evaluation using SMOS retrieved soil moisture, Journal of
732 Hydrology, 529, 200-212, 2015.

733 Stéfanon, M., Drobinski, P., D'Andrea, F., Lebeaupin-Brossier, C., and Bastin, S.: Soil moisture-
734 temperature feedbacks at meso-scale during summer heat waves over Western Europe, Climate
735 dynamics, 42, 1309-1324, 2014.

736 Temimi, M., Leconte, R., Chaouch, N., Sukumal, P., Khanbilvardi, R., and Brissette, F.: A
737 combination of remote sensing data and topographic attributes for the spatial and temporal
738 monitoring of soil wetness, Journal of Hydrology, 388, 28-40, 2010.

739 Thompson, G., Field, P. R., Rasmussen, R. M., and Hall, W. D.: Explicit forecasts of winter
740 precipitation using an improved bulk microphysics scheme. Part II: Implementation of a new snow
741 parameterization, Monthly Weather Review, 136, 5095-5115, 2008.

742 Tsai, T.-L., and Chen, H.-F.: Effects of degree of saturation on shallow landslides triggered by
743 rainfall, Environmental Earth Sciences, 59, 1285-1295, 2010.

744 Valenzuela, P., Domínguez-Cuesta, M. J., García, M. A. M., and Jiménez-Sánchez, M.: Rainfall
745 thresholds for the triggering of landslides considering previous soil moisture conditions (Asturias,
746 NW Spain), Landslides, 15, 273-282, 2018.

747 Van Den Broeke, M. S., Kalin, A., Alavez, J. A. T., Oglesby, R., Hu, Q. J. T., and climatology, a.:
748 A warm-season comparison of WRF coupled to the CLM4. 0, Noah-MP, and Bucket hydrology
749 land surface schemes over the central USA, 134, 801-816, 2018.

750 Wei, J., Dirmeyer, P. A., Guo, Z., Zhang, L., and Misra, V.: How much do different land models
751 matter for climate simulation? Part I: Climatology and variability, Journal of Climate, 23, 3120-
752 3134, 2010.

753 Wharton, S., Simpson, M., Osuna, J., Newman, J., and Biraud, S.: Assessment of Land Surface
754 Model Performance in WRF for Simulating Wind at Heights Relevant to the Wind Energy
755 Community, Lawrence Livermore National Lab (LLNL), Livermore, CA (United States), 2013.

756 Wilks, D.: Statistical Methods in the Atmospheric Sciences, 3rd ed., Academic Press, 2011.

757 Yang, Z. L., Niu, G. Y., Mitchell, K. E., Chen, F., Ek, M. B., Barlage, M., Longuevergne, L.,
758 Manning, K., Niyogi, D., and Tewari, M.: The community Noah land surface model with
759 multiparameterization options (Noah-MP): 2. Evaluation over global river basins, Journal of
760 Geophysical Research: Atmospheres, 116, 2011.

761 Zaidi, S. M., and Gisen, J. I. A.: Evaluation of Weather Research and Forecasting (WRF)
762 Microphysics single moment class-3 and class-6 in Precipitation Forecast, MATEC Web of
763 Conferences, 2018, 03007,

764 Zaitchik, B. F., Santanello, J. A., Kumar, S. V., and Peters-Lidard, C. D.: Representation of soil
765 moisture feedbacks during drought in NASA unified WRF (NU-WRF), Journal of
766 Hydrometeorology, 14, 360-367, 2013.

767 Zeng, X., and Decker, M.: Improving the numerical solution of soil moisture–based Richards
768 equation for land models with a deep or shallow water table, Journal of Hydrometeorology, 10,
769 308-319, 2009.

770 Zhao, B., Dai, Q., Han, D., Dai, H., Mao, J., and Zhuo, L.: Antecedent wetness and rainfall
771 information in landslide threshold definition, Hydrol. Earth Syst. Sci. Discuss., 2019, 1-26,
772 10.5194/hess-2019-150, 2019a.

773 Zhao, B., Dai, Q., Han, D., Dai, H., Mao, J., and Zhuo, L. J. J. o. H.: Probabilistic thresholds for
774 landslides warning by integrating soil moisture conditions with rainfall thresholds, 574, 276-287,
775 2019b.

776 Zhuo, L., Dai, Q., and Han, D.: Evaluation of SMOS soil moisture retrievals over the central United
777 States for hydro-meteorological application, Physics and Chemistry of the Earth, Parts A/B/C, 83,
778 146-155, 2015a.

779 Zhuo, L., Han, D., Dai, Q., Islam, T., and Srivastava, P. K.: Appraisal of NLDAS-2 multi-model
780 simulated soil moistures for hydrological modelling, Water resources management, 29, 3503-3517,
781 2015b.

782 Zhuo, L., Dai, Q., Han, D., Chen, N., Zhao, B., and Berti, M.: Evaluation of remotely sensed soil
783 moisture for landslide hazard assessment, IEEE Journal of Selected Topics in Applied Earth
784 Observations and Remote Sensing, 12, 162 - 173, 2019.

785

**Table 1.** Comparison of Noah, Noah-MP, and CLM4.

| | Noah | Noah-MP | CLM4 |
|---|---|---|---|
| Energy balance | Yes | Yes | Yes |
| Water balance | Yes | Yes | Yes |
| No. of soil layers | 4 | 4 | 10 |
| Depth of total soil column | 2.0 m | 2.0 m | 3.802 m |
| Model soil layer thickness | 0.1, 0.3, 0.6, 1.0 m | 0.1, 0.3, 0.6, 1.0 m | 0.018, 0.028, 0.045, 0.075, 0.124, 0.204, 0.336, 0.553, 0.913, 1.506 m |
| No. of vegetation layers | A single combined surface layer of vegetation and snow | Single layer | Single layer |
| Vegetation | Dominant vegetation type in one grid cell with prescribed LAI | Dominant vegetation type in one grid cell with dynamic LAI | Up to 10 vegetation types in one grid cell with prescribed LAI |
| No. of snow layers | A single combined surface layer of vegetation and snow | Up to three layers | Up to five layers |

**Table 2.** WRF parameterizations used in this study.

| | Settings/ Parameterizations | References |
|---|---|---|
| Map projection | Lambert | |
| Central point of domain | Latitude: 44.54; Longitude: 11.02 | |
| Latitudinal grid length | 5 km | |
| Longitudinal grid length | 5 km | |
| Model output time step | Daily | |
| Nesting | Two-way | |
| Land surface model | Noah, Noah-MP, CLM | |
| Simulation period | 1/1/2006 – 31/12/2015 | |
| Spin-up period | 1/1/2005 – 31/12/2005 | |
| Microphysics | New Thompson | (Thompson et al., 2008) |
| Shortwave radiation | Dudhia scheme | (Dudhia, 1989) |
| Longwave radiation | Rapid Radiative Transfer Model | (Mlawer et al., 1997) |
| Surface layer | Revised MM5 | (Jiménez et al., 2012;Chen and Dudhia, 2001) |
| Planetary boundary layer | Yonsei University method | (Hong et al., 2006) |
| Cumulus Parameterization | Kain-Fritsch (new Eta) scheme | (Kain, 2004) |

**Table 3.** Statistical summary of the WRF performance in simulating soil moisture for different soil layers, based on comparison with the single point in-situ observations.

| | *R* | | | | *RMSE* ($m^3/m^3$) | | | |
|---|---|---|---|---|---|---|---|---|
| | 0.10 m | 0.25 m | 0.70 m | 1.50 m | 0.1 m | 0.25 m | 0.70 m | 1.50 m |
| Noah | 0.728 | 0.645 | 0.660 | 0.430 | 0.123 | 0.125 | 0.141 | **0.055** |
| Noah-MP | **0.809** | 0.683 | **0.738** | **0.498** | **0.060** | **0.070** | **0.088** | 0.092 |
| CLM | 0.789 | **0.743** | 0.648 | 0.287 | 0.089 | 0.087 | 0.123 | 0.089 |

**Table 4**. Statistical summary of the WRF performance in simulating rainfall for the whole study region, based on comparison with the in-situ rainfall network.

| | *R* | | | *RMSE (mm)* | | |
|---|---|---|---|---|---|---|
| | Noah | Noah-MP | CLM4 | Noah | Noah-MP | CLM4 |
| Min | 0.094 | 0.090 | 0.076 | 4.275 | 4.286 | 4.219 |
| Max | 0.779 | 0.798 | 0.801 | 19.814 | 19.178 | 19.476 |
| Mean | 0.425 | 0.426 | 0.421 | 7.772 | 7.719 | 7.943 |
| 0.25 percentile | 0.147 | 0.130 | 0.154 | 4.579 | 4.297 | 4.438 |
| 0.50 percentile | 0.189 | 0.153 | 0.210 | 4.951 | 4.909 | 4.910 |
| 0.75 percentile | 0.192 | 0.183 | 0.211 | 5.006 | 4.970 | 5.010 |

**Table 5.** Rainfall events information.

| Starting date | | | Ending date | | | Duration (days) | Rainfall intensity (mm/day) | Number of Landslide events |
|---|---|---|---|---|---|---|---|---|
| Year | Month | Day | Year | Month | Day | | | |
| 2014 | 1 | 13 | 2014 | 1 | 24 | 12 | 20.50 | 2 |
| 2014 | 1 | 28 | 2014 | 2 | 14 | 18 | 13.61 | 0 |
| 2014 | 2 | 26 | 2014 | 3 | 6 | 9 | 13.35 | 0 |
| 2014 | 3 | 22 | 2014 | 3 | 27 | 6 | 11.08 | 0 |
| 2014 | 4 | 4 | 2014 | 4 | 5 | 2 | 18.98 | 0 |
| 2014 | 4 | 27 | 2014 | 5 | 4 | 8 | 12.13 | 0 |
| 2014 | 5 | 26 | 2014 | 6 | 3 | 9 | 5.05 | 0 |
| 2014 | 6 | 14 | 2014 | 6 | 16 | 3 | 18.29 | 0 |
| 2014 | 6 | 25 | 2014 | 6 | 30 | 6 | 11.39 | 0 |
| 2014 | 7 | 7 | 2014 | 7 | 14 | 8 | 7.84 | 0 |
| 2014 | 7 | 21 | 2014 | 7 | 30 | 10 | 15.35 | 0 |
| 2014 | 8 | 31 | 2014 | 9 | 5 | 6 | 5.67 | 0 |
| 2014 | 9 | 10 | 2014 | 9 | 12 | 3 | 11.84 | 0 |
| 2014 | 9 | 19 | 2014 | 9 | 20 | 2 | 23.04 | 0 |
| 2014 | 10 | 1 | 2014 | 10 | 1 | 1 | 14.51 | 0 |
| 2014 | 10 | 10 | 2014 | 10 | 17 | 8 | 13.01 | 0 |
| 2014 | 11 | 4 | 2014 | 11 | 18 | 15 | 18.28 | 0 |
| 2014 | 11 | 25 | 2014 | 12 | 7 | 13 | 7.58 | 0 |
| 2014 | 12 | 13 | 2014 | 12 | 16 | 4 | 6.24 | 0 |
| 2015 | 1 | 16 | 2015 | 1 | 17 | 2 | 14.87 | 0 |
| 2015 | 1 | 21 | 2015 | 1 | 23 | 3 | 7.13 | 0 |
| 2015 | 1 | 29 | 2015 | 2 | 10 | 13 | 9.98 | 0 |
| 2015 | 2 | 13 | 2015 | 2 | 17 | 5 | 6.62 | 1 |
| 2015 | 2 | 21 | 2015 | 2 | 26 | 6 | 11.84 | 4 |
| 2015 | 3 | 3 | 2015 | 3 | 7 | 5 | 11.69 | 1 |
| 2015 | 3 | 15 | 2015 | 3 | 17 | 3 | 9.00 | 0 |
| 2015 | 3 | 21 | 2015 | 3 | 27 | 7 | 12.09 | 2 |
| 2015 | 4 | 3 | 2015 | 4 | 5 | 3 | 16.62 | 0 |
| 2015 | 4 | 17 | 2015 | 4 | 18 | 2 | 6.99 | 0 |
| 2015 | 4 | 26 | 2015 | 4 | 29 | 4 | 11.23 | 0 |
| 2015 | 5 | 15 | 2015 | 5 | 16 | 2 | 8.83 | 0 |
| 2015 | 5 | 20 | 2015 | 5 | 27 | 8 | 10.58 | 1 |
| 2015 | 6 | 8 | 2015 | 6 | 11 | 4 | 6.47 | 0 |
| 2015 | 6 | 16 | 2015 | 6 | 19 | 4 | 13.44 | 0 |
| 2015 | 6 | 23 | 2015 | 6 | 24 | 2 | 6.07 | 0 |
| 2015 | 7 | 22 | 2015 | 7 | 25 | 4 | 6.05 | 0 |
| 2015 | 8 | 9 | 2015 | 8 | 10 | 2 | 24.69 | 0 |
| 2015 | 8 | 15 | 2015 | 8 | 19 | 5 | 10.69 | 0 |
| 2015 | 8 | 23 | 2015 | 8 | 24 | 2 | 7.88 | 0 |
| 2015 | 9 | 13 | 2015 | 9 | 14 | 2 | 24.66 | 1 |
| 2015 | 9 | 23 | 2015 | 9 | 24 | 2 | 7.50 | 0 |
| 2015 | 10 | 1 | 2015 | 10 | 7 | 7 | 13.73 | 0 |
| 2015 | 10 | 10 | 2015 | 10 | 19 | 10 | 9.40 | 0 |
| 2015 | 10 | 27 | 2015 | 10 | 29 | 3 | 20.33 | 0 |
| 2015 | 11 | 21 | 2015 | 11 | 25 | 5 | 13.78 | 1 |

**Table 6.** Results of Euclidean distances (*d*) between individual points and the optimal point for ROC analysis are listed. The best performance (i.e., lowest *d*) for each column (i.e., each soil layer of an LSM scheme) is highlighted. The optimal performance of all is highlighted in red.

| | Noah | | | | Noah-MP | | | | CLM4 | | | |
|---|---|---|---|---|---|---|---|---|---|---|---|---|
| *e.p. (%).* | 10 cm | 25 cm | 70 cm | 150 cm | 10 cm | 25 cm | 70 cm | 150 cm | 10 cm | 25 cm | 70 cm | 150 cm |
| 1 | 0.942 | 0.971 | 0.962 | 0.947 | 0.857 | 0.937 | 0.897 | 0.963 | 0.942 | 0.939 | 0.978 | 0.975 |
| 2 | 0.906 | 0.945 | 0.963 | 0.923 | 0.854 | 0.912 | 0.883 | 0.959 | 0.923 | 0.922 | 0.959 | 0.952 |
| 3 | 0.889 | 0.924 | 0.961 | 0.915 | 0.849 | 0.855 | 0.838 | 0.952 | 0.870 | 0.874 | 0.940 | 0.947 |
| 4 | 0.884 | 0.898 | 0.946 | 0.914 | 0.838 | 0.814 | 0.829 | 0.924 | 0.831 | 0.843 | 0.925 | 0.947 |
| 5 | 0.860 | 0.875 | 0.924 | 0.896 | 0.820 | 0.793 | 0.812 | 0.908 | 0.791 | 0.822 | 0.915 | 0.921 |
| 6 | 0.835 | 0.854 | 0.910 | 0.874 | 0.803 | 0.785 | 0.800 | 0.905 | 0.770 | 0.817 | 0.911 | 0.909 |
| 7 | 0.827 | 0.861 | 0.902 | 0.858 | 0.777 | 0.767 | 0.791 | 0.889 | 0.753 | 0.801 | 0.902 | 0.900 |
| 8 | 0.816 | 0.849 | 0.889 | 0.851 | 0.745 | 0.765 | 0.782 | 0.876 | 0.745 | 0.785 | 0.902 | 0.910 |
| 9 | 0.790 | 0.827 | 0.878 | 0.834 | 0.706 | 0.732 | 0.766 | 0.871 | 0.742 | 0.777 | 0.864 | 0.904 |
| 10 | 0.762 | 0.811 | 0.863 | 0.825 | 0.672 | 0.702 | 0.747 | 0.862 | 0.738 | 0.767 | 0.835 | 0.887 |
| 15 | 0.615 | 0.741 | 0.839 | 0.763 | 0.560 | 0.629 | 0.716 | 0.835 | 0.702 | 0.700 | 0.729 | 0.790 |
| 20 | 0.485 | 0.627 | 0.779 | 0.652 | 0.515 | 0.571 | 0.624 | 0.774 | 0.570 | 0.602 | 0.594 | 0.650 |
| 25 | 0.432 | 0.544 | 0.728 | 0.512 | 0.403 | 0.465 | 0.574 | 0.736 | 0.509 | 0.522 | 0.471 | 0.509 |
| 30 | 0.437 | 0.495 | 0.643 | 0.451 | **0.369** | **0.375** | 0.544 | 0.679 | 0.475 | 0.477 | 0.447 | 0.469 |
| 35 | **0.392** | 0.446 | 0.592 | 0.436 | 0.390 | 0.404 | 0.411 | 0.498 | 0.441 | 0.435 | 0.428 | 0.430 |
| 40 | 0.500 | **0.407** | 0.531 | 0.416 | 0.439 | 0.385 | **0.382** | 0.436 | **0.406** | **0.405** | **0.398** | **0.410** |
| 50 | 0.552 | 0.425 | **0.404** | **0.411** | 0.489 | 0.417 | 0.416 | **0.429** | 0.437 | 0.435 | 0.408 | 0.437 |

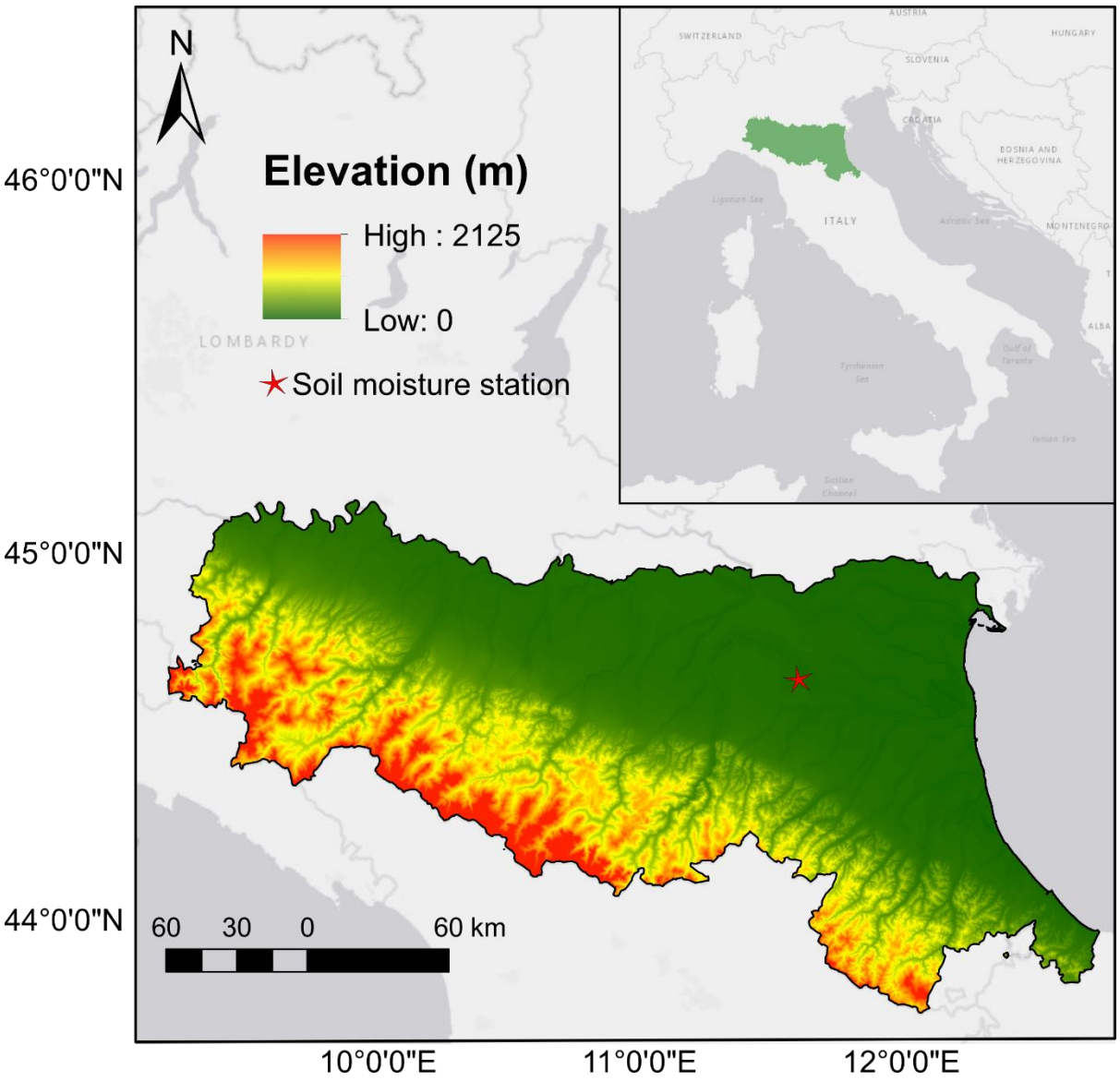


**Figure 1.** Location of the Emilia Romagna Region with elevation map and in-situ soil moisture station also shown.

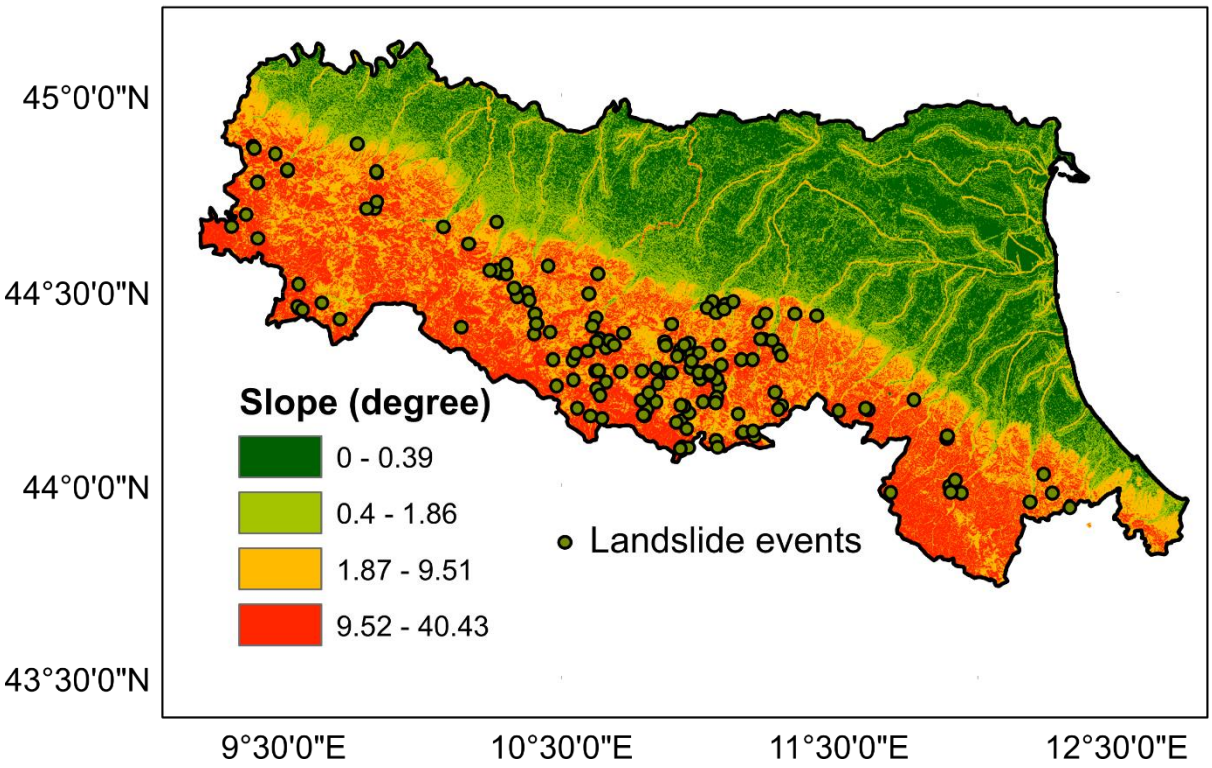


**Figure 2.** Landslide events with slope angle map.

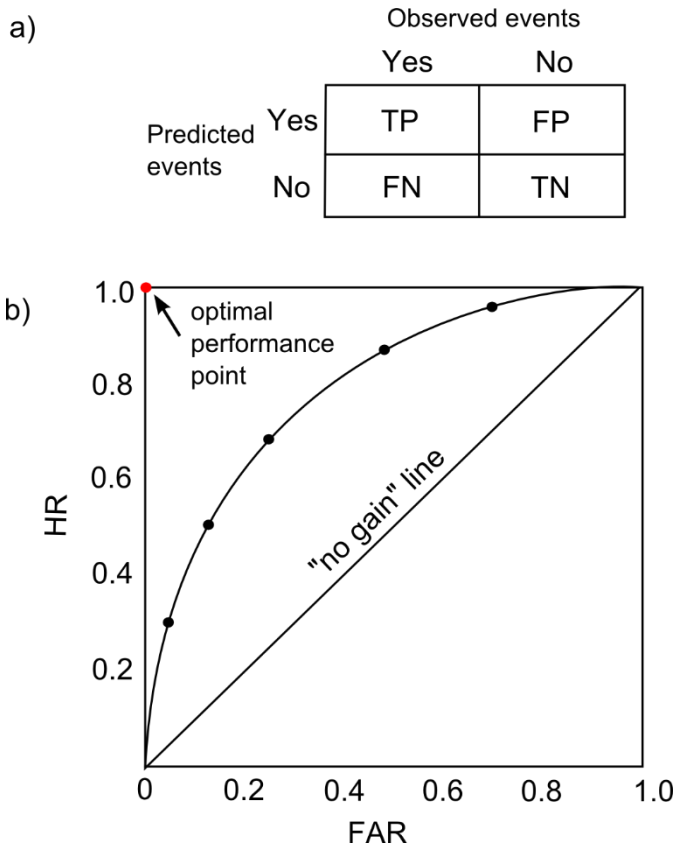


**Figure 3.** a) Contingency table illustrates the four possible outcomes of a binary classifier model: TP (True Positive), TN (True Negative), FP (False Positive), and FN (False Negative). b) ROC (Receiver Operating Characteristic) analysis with HR (Hitting Rate) against FAR (False Alarm Rate).

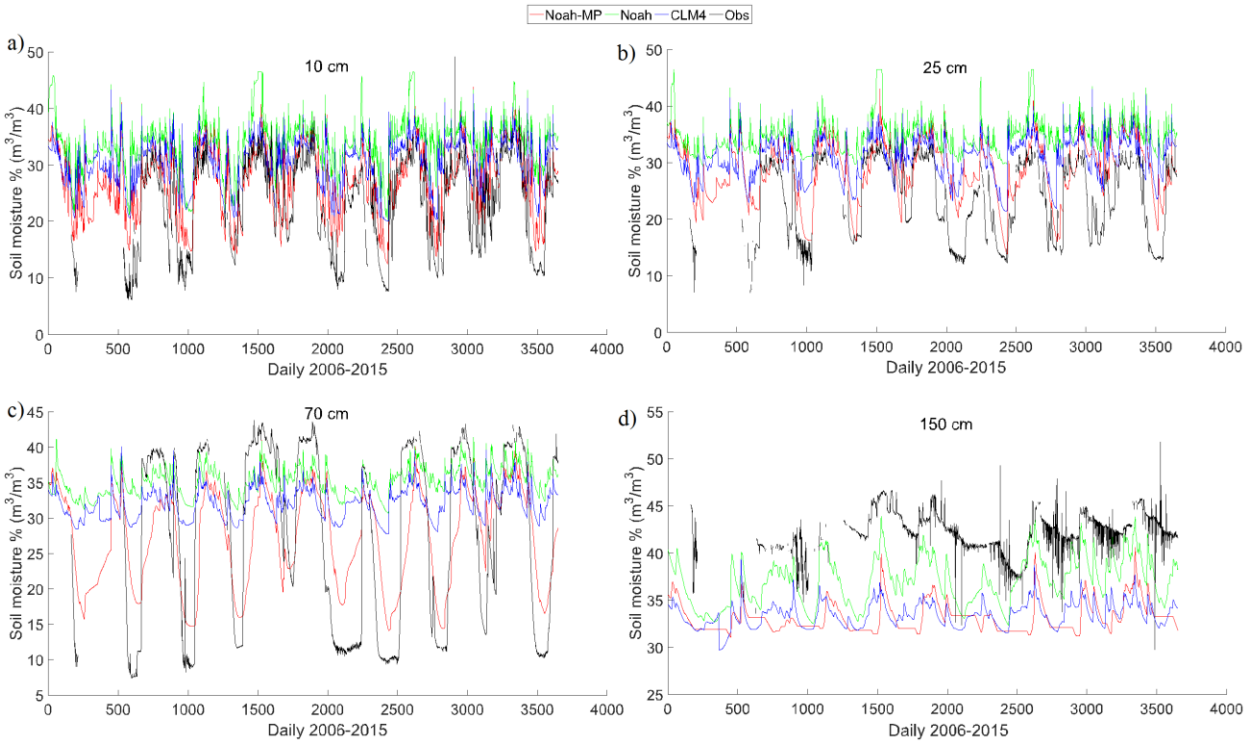


**Figure 4.** Soil moisture temporal variations of WRF simulations and in-situ observations for four soil layers at a) 10 cm; b) 25 cm; c) 70 cm; and d) 150 cm.

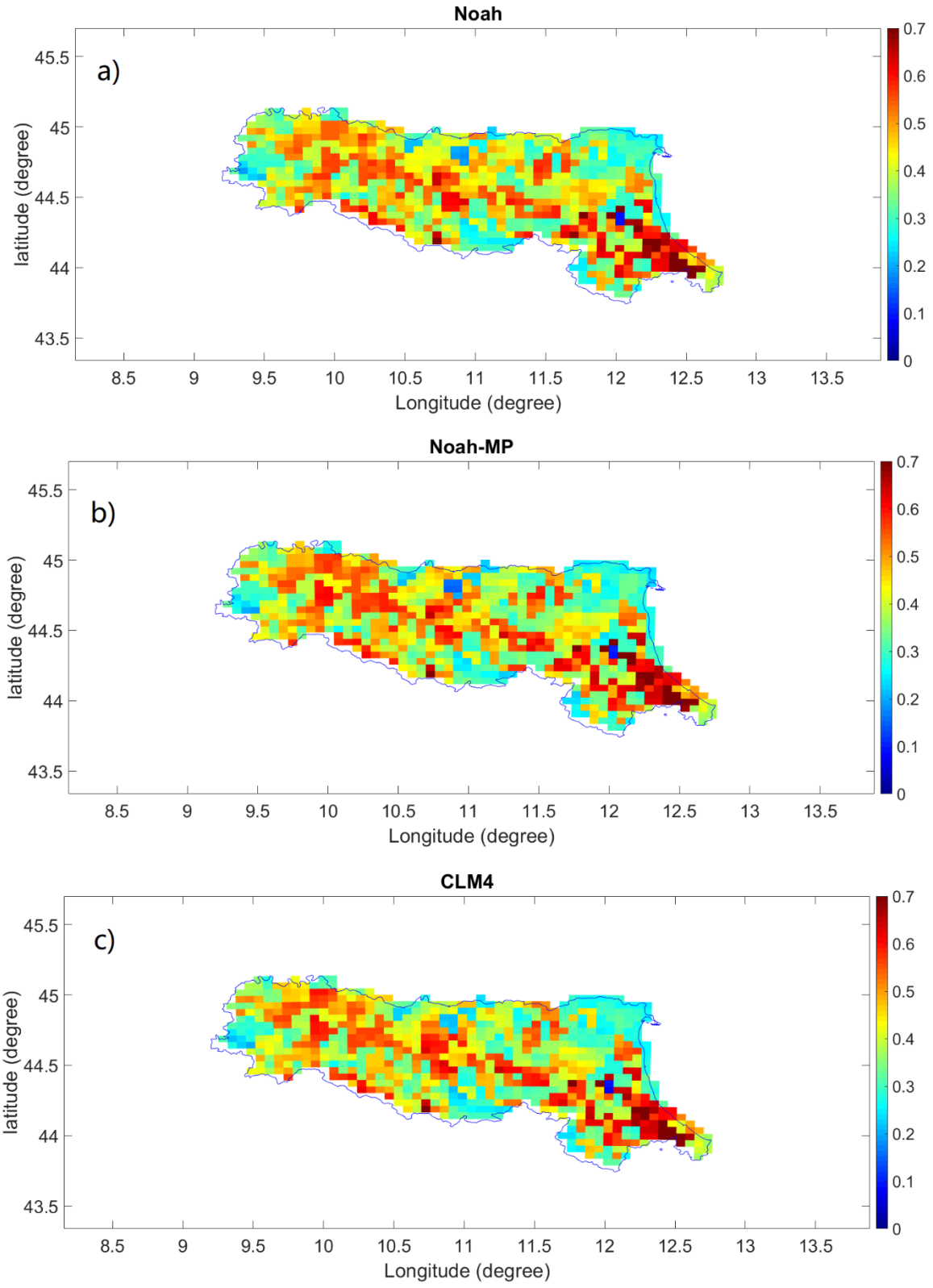


**Figure 5.** Rainfall evaluation: spatial distribution of the correlation coefficient *R* of a) Noah, b) Noah-MP and c) CLM4.

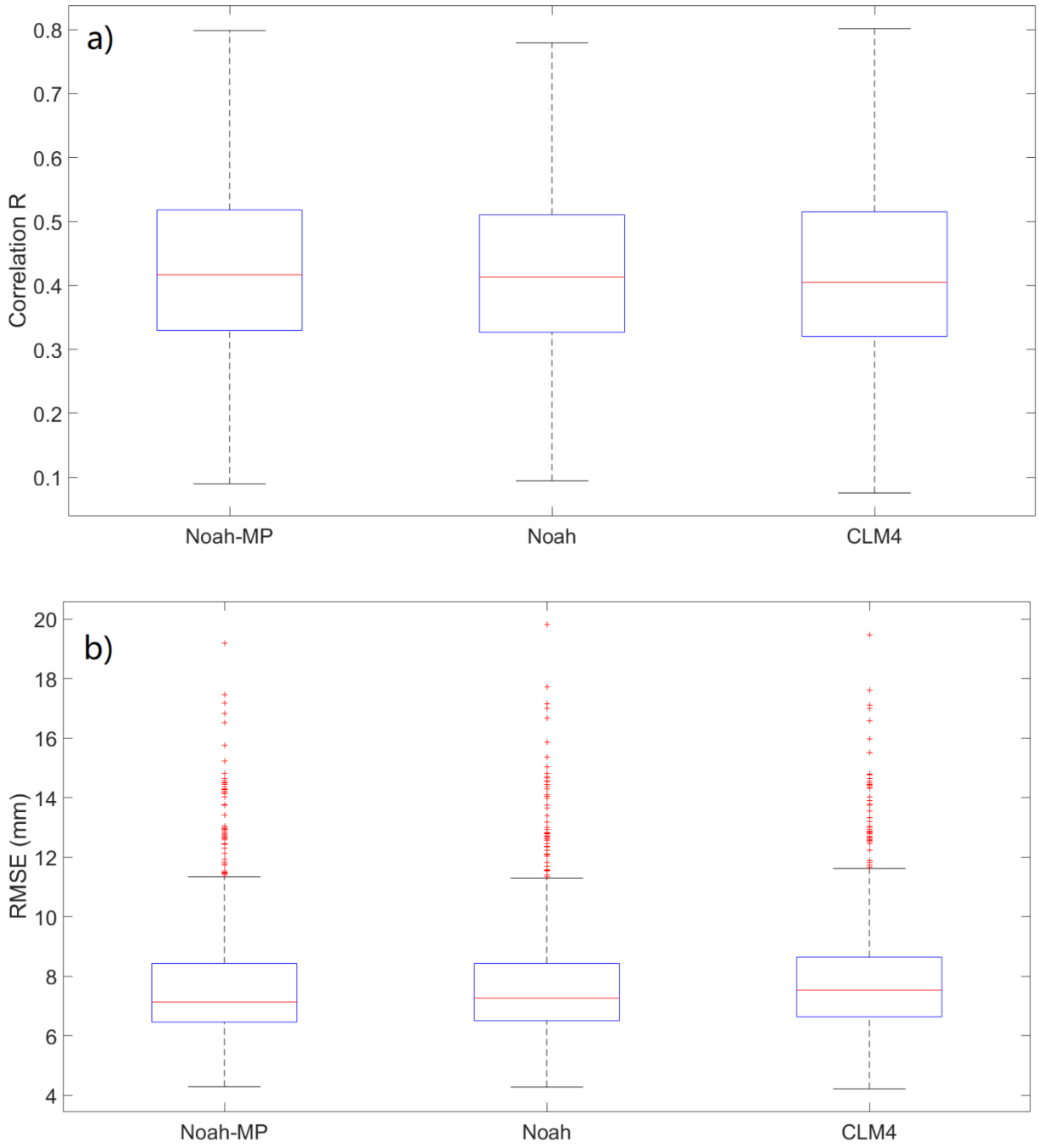


**Figure 6.** Boxplots of rainfall evaluation results of a) *R* and b) *RMSE*: minimum, maximum, 0.25, 0.50 and 0.75 percentiles, and outliers (red cross).

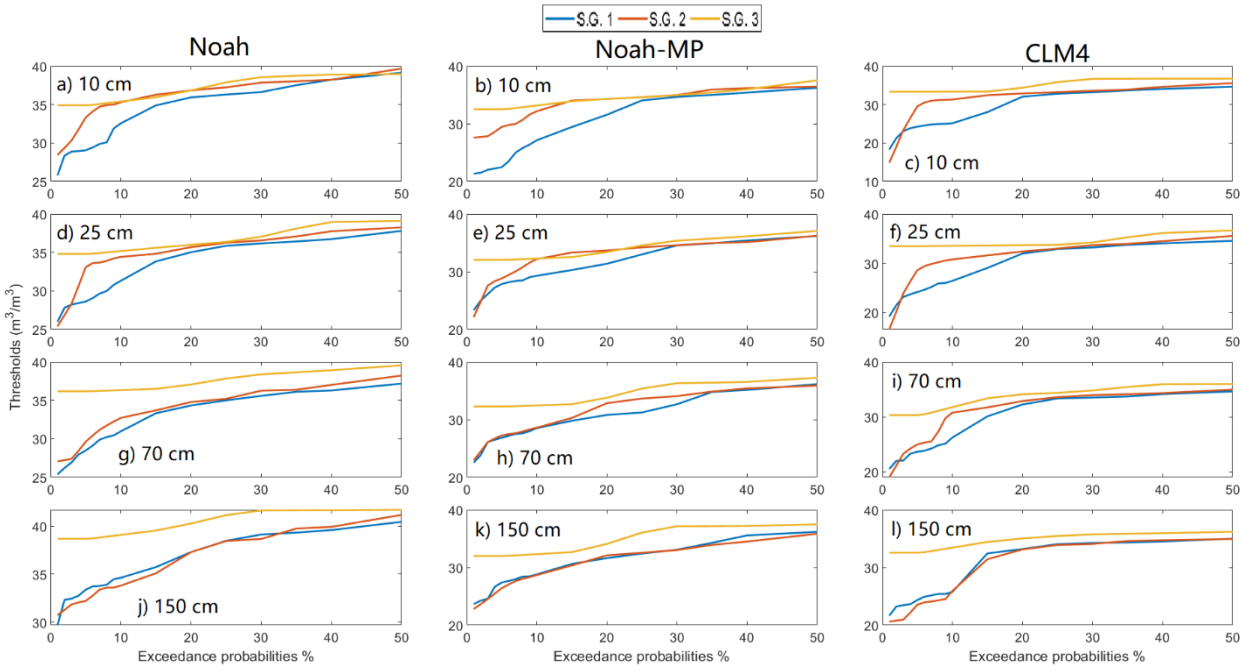


**Figure 7.** Threshold plots. For Noah (a, d, g, j), Noah-MP (b, e, h, k), and CLM4 (c, f, i, l) land surface schemes under three Slope angle Groups (S.G.) with S.G. 1 = 0.4-1.86º; S.G. 2 = 1.87-9.61º; S.G. 3 = 9.52-40.43º.

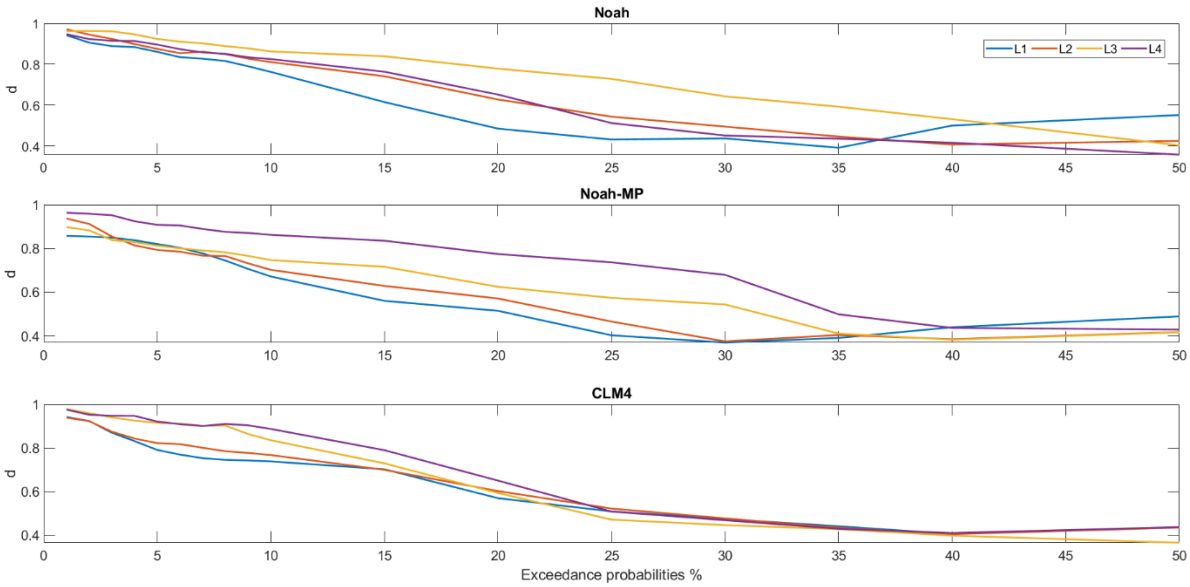


**Figure 8.** d-scores.

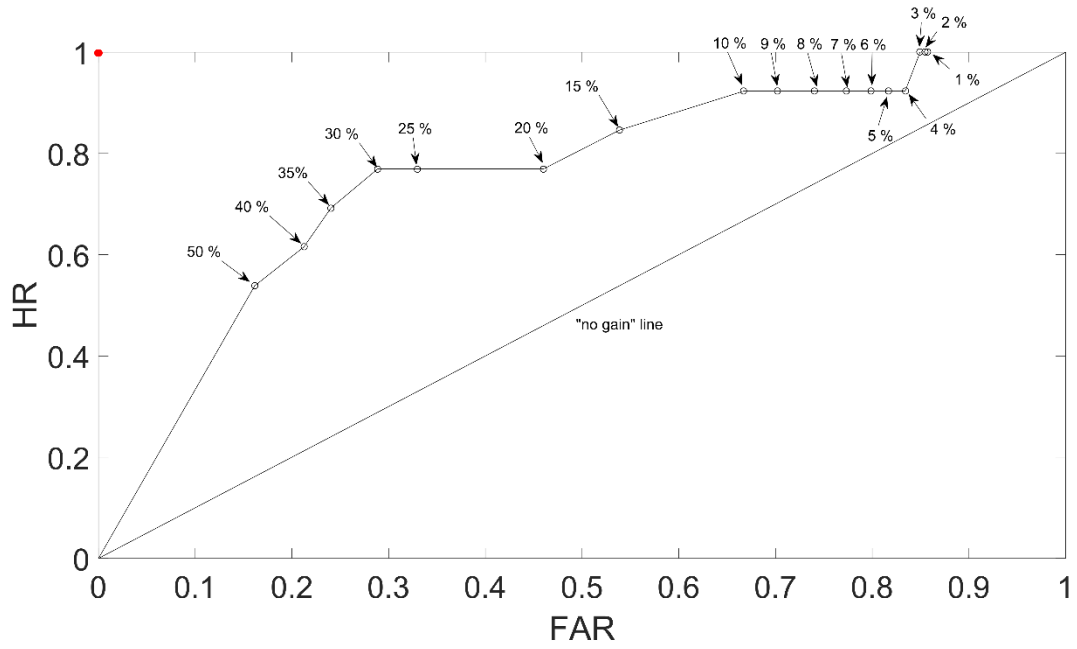


**Figure 9.** ROC curve for the calculated thresholds using different exceedance probability levels (for Noah-MP at the surface layer). The *no gain* line and the optimal performance point (the red point) are also presented.

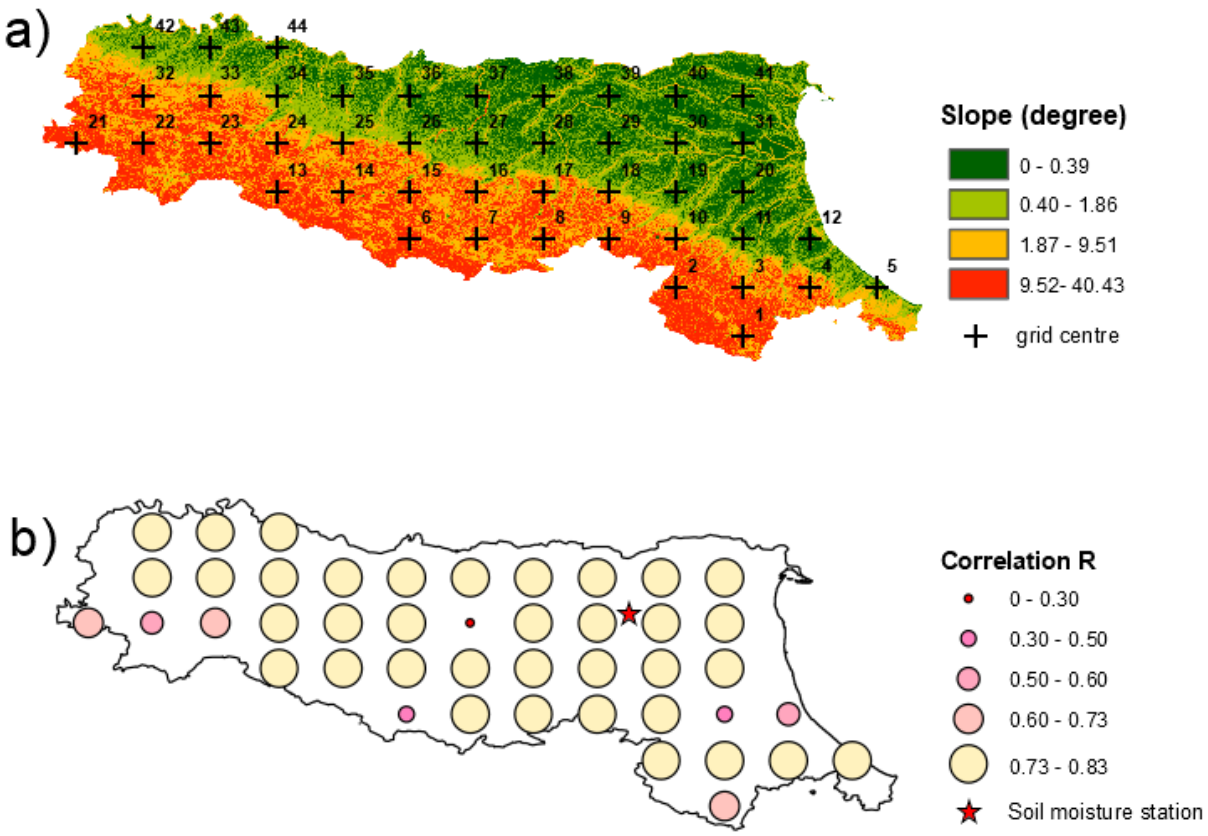


**Figure 10.** The cross-validation of spatially distributed WRF soil moisture against the in-situ soil moisture observation at the single point soil moisture sensor in plain area: a) grid numbers shown on the slope map, b) correlation spatial performance.

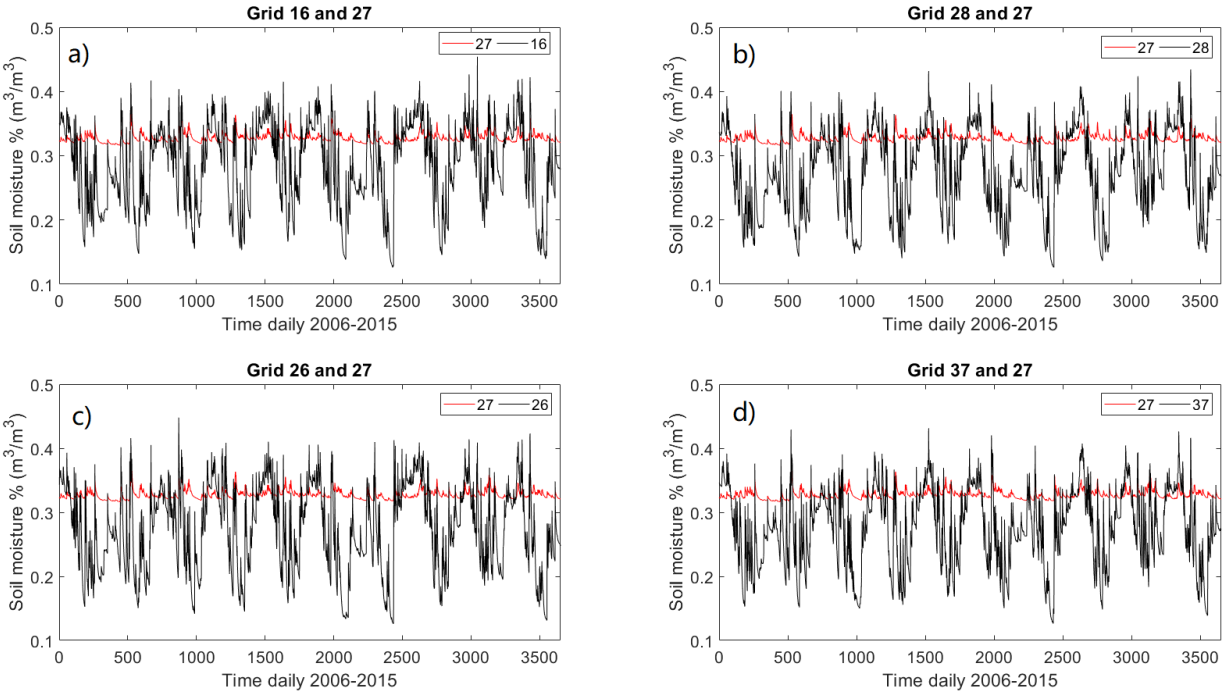


**Figure 11.** The soil moisture comparisons of Grid 27 with the adjacent grids (16, 28, 26, 37).